TAMPEREEN TEKNILLINEN YLIOPISTO
TAMPERE UNIVERSITY OF TECHNOLOGY

Suvi Lehtimäki

Printed Supercapacitors for Energy Harvesting Applications

Julkaisu 1463 • Publication 1463

Tampere 2017

Tampereen teknillinen yliopisto. Julkaisu 1463
Tampere University of Technology. Publication 1463

Suvi Lehtimäki

Printed Supercapacitors for Energy Harvesting Applications

Thesis for the degree of Doctor of Science in Technology to be presented with due permission for public examination and criticism in Rakennustalo Building, Auditorium RG202, at Tampere University of Technology, on the 7th of April 2017, at 12 noon.

Tampereen teknillinen yliopisto - Tampere University of Technology
Tampere 2017

Doctoral candidate: Suvi Lehtimäki, M.Sc.
Department of Electronics and Communications Engineering
Tampere University of Technology

Supervisors: Donald Lupo, Prof.
Laboratory for Future Electronics
Department of Electronics and Communications Engineering
Tampere University of Technology

Sampo Tuukkanen, Asst. Prof.
Department of Automation Science and Engineering
Tampere University of Technology

Pre-examiners: Olli Ikkala, Prof.
Department of Applied Physics
Aalto University

Li-Rong Zheng, Prof.
School of Information and Communication Technology
KTH Royal Institute of Technology

Opponent: Leif Nyholm, Prof.
Department of Chemistry
Uppsala University

Painopaikka:
Juvenes Print
Suomen Yliopistopaino Oy
Tampere 2017

ISBN 978-952-15-3922-0 (printed)
ISBN 978-952-15-3927-5 (PDF)
ISSN 1459-2045

Abstract

Energy harvesting from ambient sources such as light or vibrations is a promising method for powering distributed and ubiquitous electronics. Harvesting requires an intermediate energy storage, for which supercapacitors are well suited due to their long cycle life compared to batteries. Moreover, supercapacitors can be prepared from non-toxic materials with printing methods, enabling their use in many applications.

This thesis analyzes different types of solution processed supercapacitors prepared using different materials, fabrication methods and architectures, and their use in energy harvesting. Supercapacitors were prepared from the conventional material, activated carbon, as well as novel materials: carbon nanotubes and conducting polymer composites. Layers were deposited by doctor blade coating and screen printing, and in the case of conducting polymers, also electrochemical deposition. Neutral aqueous electrolytes were used in the supercapacitors.

Carbon nanotubes (CNTs), which have both conductivity and a high surface area, offer the possibility of preparing the supercapacitor electrodes with only one layer, without a separate current collector. In this work, CNT supercapacitors were prepared from blade-coated electrodes, and capacitances of $6\,\mathrm{mF/cm^2}$ were achieved. The equivalent series resistance (ESR) was large, $80\,\Omega$, probably due to the large amount of dispersant polymer needed in the ink. The other novel material studied in this work was a composite of poly(3,4-ethylenedioxythiophene) (PEDOT) and reduced graphene oxide. Symmetric supercapacitors prepared from electropolymerized layers on plastic substrates yielded $18\,\mathrm{mF/cm^2}$ capacitance and $25\,\Omega$ ESR. It was found that the reduced graphene oxide accounts for approximately 30% of the capacitance of the composite, although morphology changes due to its incorporation have an effect as well.

Screen-printed supercapacitors were prepared from a graphite ink as a current collector and an activated carbon based ink as the active layer. The effect of varying layer thicknesses on the device properties was examined in detail. On average, capacitance of $150\,\mathrm{mF/cm^2}$ and ESR of $10\,\Omega$ was achieved and the current collectors were found to be the main source of the ESR. The effect of the maximum voltage on the device properties was also tested, and while a higher voltage yielded a higher capacitance, it also led to a higher leakage current as well as quicker device degradation. Based on these results, $1.0\,\mathrm{V}$ was found to be a good compromise for the maximum voltage of the supercapacitors.

Energy harvesting was demonstrated with a printed radio-frequency harvester. Using two $450\,\mathrm{mF}$ supercapacitors in series, a $1.2\,\mathrm{V}$ voltage-control circuit could be operated for over 10 hours with a steady output. Operating an electrochromic display was also demonstrated with a supercapacitor charged through a solar cell module under ambient lighting.

Preface

This work was carried out at the Department of Electronics and Communications Engineering at Tampere University of Technology. The research was funded by the Academy of Finland, the Finnish Funding Agency for Technology and Innovation (Tekes), and Jenny and Antti Wihuri Foundation. The work was also supported by Tekniikan edistämissäätiö and the Nokia Foundation.

I would like to thank my supervisor, Prof. Donald Lupo, for his guidance throughout my work. I am also grateful to my co-supervisor Asst. Prof. Sampo Tuukkanen for his support. I would like to thank my past and present colleagues in the Laboratory for Future Electronics for the great working atmosphere; in particular I thank D.Sc. Marika Janka, D.Sc. Petri Heljo and M.Sc. Anna Railanmaa for the many helpful and pleasant conversations. I also wish to thank my colleagues M.Sc. Miao Li, M.Sc. Juho Pörhönen, and Lic.Sc. Jari Keskinen, as well as M.Sc. Milla Suominen, Docent Pia Damlin and Prof. Carita Kvarnström of Turku University, as my work would not have been finished without their invaluable help.

Finally, I thank my family for their love and support through the years. I especially want to thank my beloved husband Jouni for always being there for me, and our daughter Sonja for bringing me great joy.

Tampere, March 2017

Suvi Lehtimäki

Contents

Abbreviations and symbols

AC	Activated carbon
ASIC	Application specific integrated circuit
CNT	Carbon nanotube
CV	Cyclic voltammetry
ECD	Electrochromic display
EDL	Electric double layer
EDLC	Electric double layer capacitor
EDS	Energy-dispersive X-ray spectroscopy
ESR	Equivalent series resistance
GCD	Galvanostatic charge-discharge
GO	Graphene oxide
OPV	Organic photovoltaic
PEDOT	Poly(3,4-ethylenedioxythiophene)
PET	Poly(ethylene terephthalate)
RF	Radio frequency
RFID	Radio frequency identification
rGO	Reduced graphene oxide
SEM	Scanning electron microscopy
TEM	Transmission electron microscopy

C	Capacitance
$\bar{C}$	Complex capacitance
C'	Real part of $\bar{C}$
C''	Imaginary part of $\bar{C}$
E	Energy
I	Electric current
Q	Electric charge
R_F	Faradaic leakage resistance
R_S	Series resistance
t	Time
τ_0	Characteristic time
V	Voltage
$\bar{Z}$	Complex impedance
Z'	Real part of $\bar{Z}$
Z''	Imaginary part of $\bar{Z}$

List of publications

I S. Lehtimäki, M. Li, J. Salomaa, J. Pörhönen, A. Kalanti, S. Tuukkanen, D. Lupo. Performance of printable supercapacitors in an RF energy harvesting circuit. *International Journal of Electrical Power & Energy Systems* 58, pp. 42–46, 2014.

II S. Lehtimäki, S. Tuukkanen, J. Pörhönen, P. Moilanen, J. Virtanen, M. Honkanen, D. Lupo. Low-cost, solution processable carbon nanotube supercapacitors and their characterization. *Applied Physics A* 117(3), pp. 1329–1334, 2014.

III S. Lehtimäki, M. Suominen, P. Damlin, S. Tuukkanen, C. Kvarnström, D. Lupo. Preparation of supercapacitors on flexible substrates with electrodeposited PEDOT/graphene composites. *ACS Applied Materials & Interfaces* 7(40), pp. 22137–22147, 2015.

IV S. Lehtimäki, A. Railanmaa, J. Keskinen, M. Kujala, S. Tuukkanen, D. Lupo. Properties and operating voltage optimization of screen-printed aqueous supercapacitors. *Accepted for publication in Scientific Reports.*

1 Introduction

It has been projected that the number of objects in the Internet of Things, wireless sensor networks and other instances of ubiquitous electronics will rise to billions in the next few years. This means "smart" devices which can sense, control and communicate in various ways, for example from wearable devices measuring body signals to those monitoring conditions in buildings. However, powering most such devices is impossible through connecting them to power outlets with wiring, and often infeasible through batteries which need to be changed or recharged regularly. A solution to this problem is the harvesting of energy from ambient light, radio frequency fields, motion or temperature gradients. Such energy "scavenging" enables the device to function for months, even years, without maintenance. [1 – 10]

The power output from harvesting sources is usually irregular and uneven. Therefore, energy storage is an essential part of any harvester system [4, 5]. Usually, the envisioned energy storage is a rechargable battery, but in some applications the toxic chemicals in them can become problematic due to safety and and disposability requirements [11]. Moreover, the cycle lifetime of batteries is often limited compared to the required lifetime for the application. An alternative to batteries is the use of supercapacitors, which store energy electrostatically. The absence of chemical reactions increases the number of charge-discharge cycles of the device drastically compared to batteries, as well as increasing the available power output [12]. Moreover, supercapacitors can be prepared from non-toxic materials, which means they can be safely used in any environment and disposed of easily [13].

The operation of supercapacitors is based on the accumulation of electrolyte ions on the surface of a porous electrode material, the most common one of which is activated carbon [12]. In most commercial supercapacitors, the electrolyte is organic, which allows the device to be used up to 2.5 – 3.0 V. Aqueous electrolytes restrict the maximum voltage of one cell to approximately 1 V, but offer other advantages such as ease of handling, low cost, environmental friendliness, and safety [14]. While commercial supercapacitors are usually produced with rigid packaging, the emergence of printed electronics has opened up the possibility of preparing small, lightweight and even flexible supercapacitors on plastic substrates through printing methods [13, 15 – 18]. Such devices are well suited for many applications of ubiquitous electronics, in particular when the electrolyte chosen is aqueous.

The main objective of this thesis is to study supercapacitors prepared from different printable and coatable materials and their use in energy harvesting applications. The microcontrollers used in embedded systems are usually designed to consume as little energy as possible: commonly, a few mA for under one second are needed in the active mode and at most 1 µA in the "sleep" mode, which is the majority of the time in most

sensor applications [4]. Thus, the capacity requirement of the energy storage is on the order of tens of millijoules, which at 1 V voltage corresponds to some tens to a hundred millifarads. Due to the linear voltage decline of capacitors on discharge, all of the stored energy cannot be utilized and the capacity needs to be somewhat higher.

The supercapacitors presented in this thesis are prepared from both conventional and novel materials. Using blade coating and screen-printing, as well as electropolymerization, devices are prepared on flexible plastic substrates. While this makes the devices also potentially flexible, that topic is a broad one including the challenges in packaging and sealing the liquid electrolyte. The detailed study of device flexibility is not within the scope of this thesis; the focus is mainly on the fabrication and performance analysis of printable supercapacitors.

The thesis outlines the work done in four peer-reviewed publications. In **I**, activated-carbon based supercapacitors are fabricated using blade-coating, characterized, and subsequently used in an energy harvesting application with a printed RF harvester. Two novel materials, carbon nanotubes and conducting polymer composites with reduced graphene oxide are explored in **II** and **III**, respectively. In the latter, a harvesting demonstration is also performed using a printed organic solar cell and an electrochromic display. Publication **IV** is a detailed look into the properties of screen printed supercapacitors, exploring the variation of the capacitance, leakage current and ESR with varying layer thicknesses, as well as looking into the effect of the maximum voltage on the properties.

Chapter 2 presents the theoretical background of the work, from the basic structure and properties of supercapacitors to the latest reports in literature on printed supercapacitors, as well as an overview of the characterization methods. The experimental methods are presented in Chapter 3, and the main results of the included publications are outlined in Chapter 4. The final chapter gives a summary of the work as well as a future outlook of the research.

Contribution of the author

The publications included in this thesis are the result of collaboration. The contribution of the author is as follows:

Publication I The author designed and fabricated the supercapacitors and performed their electrical characterization. Miao Li prepared the printed harvester at TUT and the ASIC was designed and fabricated at Aalto University. The author planned and performed the harvesting measurements together with M. Li. The author analyzed the measurement data and wrote the first version of the manuscript.

Publication II The author planned the experiment and fabricated and characterized the supercapacitors from the ink which was obtained from collaborators. The author built the simulation model and analyzed the measurement and simulation data. The author wrote the first version of the manuscript.

Publication III The author prepared the current collector electrodes, on which the active layers were fabricated at the University of Turku. The author assembled supercapacitors and performed their basic characterization and data analysis. The author performed the harvesting experiment together with S. Tuukkanen. The author analyzed the results and wrote the first version of the manuscript.

Publication IV The author planned the experiments and fabricated most of the samples. The author performed the characterization, analyzed the data and wrote the first version of the manuscript.

2 Background

2.1 Basic principles of supercapacitors

Supercapacitors are energy storage devices whose properties are between those of batteries and capacitors. While the energy that can be stored in a supercapacitor is lower than in a battery, the power capability is much larger. Supercapacitors store energy in an electrostatic manner, without electrochemical reactions and phase changes, and as a result, the cyclability and reliability of the devices is better than that of batteries. Compared to regular capacitors, which can provide even higher power peaks, the energy which can be stored in supercapacitors is high: common device capacitances are many orders of magnitude larger than in regular capacitors, ranging from 1 to several thousand farads. [12]

Thus, supercapacitors bridge the gap between batteries and capacitors and can be utilized in many applications where large power peaks and longer cycle lives are required. These include short-term power backup, engine ignition, portable tools and regenerative braking in vehicles. Supercapacitors can also be used in combination with batteries to achieve both high energy and high power capabilities; an example is electric vehicles where supercapacitors are able to deliver short bursts of high power as well as store braking energy. Using only batteries, covering the power peaks would require a greatly oversized battery. [19]

2.1.1 Structure

Supercapacitors consist of two electrodes with an electrolyte and a separator film between them (Fig. 2.1). The electrodes are porous with a high surface area, usually composed of activated carbon. When a voltage is applied between the electrodes, ions in the electrolyte move and form *electric double layers* (EDL), in which the charge in the electrode is compensated for by a layer of oppositely charged ions on the surface. The voltage must be kept below the limit for any electrochemical reactions to occur, so that the ions are accumulated electrostatically on the electrode surface. The double layer on each electrode essentially forms a plate capacitor with the distance between the charged layers in molecular dimensions. As the capacitance of a plate capacitor is inversely proportional to this distance, the resulting capacitance is very large. The capacitance is further increased by the large surface area of the porous electrode material. [12, 20]

In a supercapacitor, the two "capacitors" of the double layer electrodes are connected in series, with the electrolyte as an ionic conductor between them. The total capacitance C is calculated from

$$\frac{1}{C} = \frac{1}{C_1} + \frac{1}{C_2}, \tag{2.1}$$

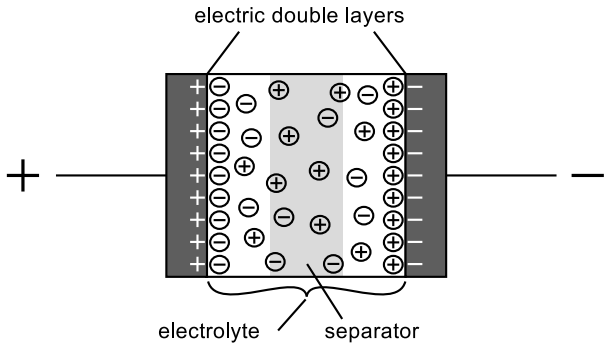

Figure 2.1: The structure of a supercapacitor

where C_1 and C_2 are the electrode capacitances. If $C_1 = C_2$, the total capacitance is half of the one-electrode capacitance. If the capacitances are unequal, the smaller one dominates the total capacitance – thus, it is important to have equal capacitances on the electrodes. Single electrode capacitances can be measured in a three-electrode cell against a reference electrode; in this case, it should be remembered that real devices will have at most half of the single-electrode capacitance. [12]

The capacitance of an active material is often given per mass as specific capacitance (F/g), which facilitates comparison of different materials. In a symmetric device, the total capacitance divided by the total active material mass is then 1/4 of the single electrode specific capacitance, because the mass is doubled and the capacitance halved due to the series connection [20]. When reporting material properties, it is important to note whether the specific capacitance is from the whole device or from single-electrode measurements.

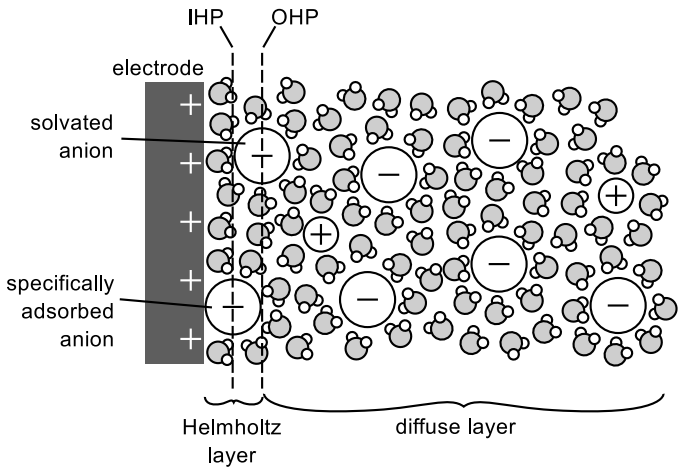

Figure 2.2: The microscopic structure of the electric double layer. OHP refers to the outer and IHP to the inner Helmholtz plane, i.e. the closest approach distance of hydrated and specifically absorbed ions, respectively.

Fig. 2.2 shows a microscopic depiction of the EDL structure. It is usually assumed that the charge in the electrode is localized very close to the surface due to the good electrical

conductivity of the material. In the solution side of the double layer, the ions spread out in a *diffuse layer*, which contains both negative and positive ionic species. Close to the electrode surface lies the *compact* or *Helmholtz* layer, which consists of ions with a charge opposite to the electrode. The closest approach plane of solvated ions – i.e., non-specifically adsorbed ions – is termed the outer Helmholz plane. Ions can also be specifically adsorbed, losing their solvation shell, with the plane through the center of these ions called the inner Helmholz plane. [12, 21]

Because the double layer ions are different on the positive and negative electrodes, the double layers and thus capacitances of the electrodes are not identical even if the electrode structure is symmetric. Usually, the anions are more strongly adsorbed due to their larger size and lower charge density, which results in a loosely-bound solvation shell; cations are usually more strongly solvated and thus are less likely to be specifically adsorbed. The difference in capacitance can be up to a factor of two. [21, 22]

2.1.2 Resistance and leakage

The electrical properties of supercapacitors can be simplified in an equivalent circuit such as that depicted in Fig. 2.3(a), where the EDL capacitance of each electrode, C_{EDL}, is accompanied by a leakage resistance due to Faradaic reactions, R_F, in parallel with the capacitance. A series resistance, R_S, represents the resistance of the electrolyte solution [12, p. 483]. The leakage eventually results in the self-discharge of the capacitor. This means that the capacitor cannot be stored in the charged state indefinitely. Supercapacitor self-discharge rates are larger than in batteries, where the mechanism is also somewhat different [12, p. 558].

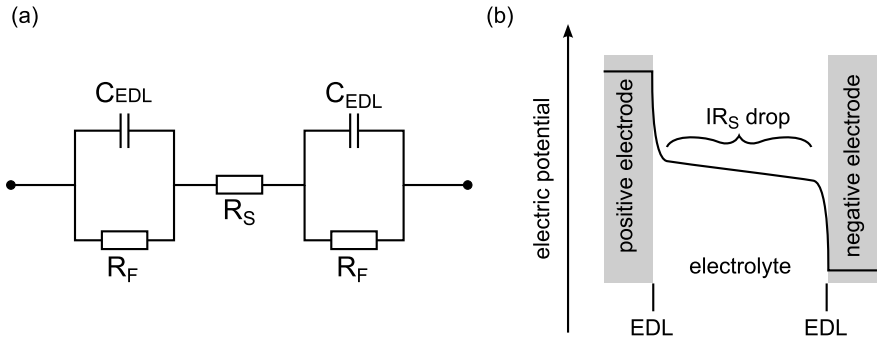

Figure 2.3: (a) An equivalent circuit describing the electrical behaviour of a supercapacitor. (b) The electrical potential in a supercapacitor when charged or discharged with a constant current I. An IR drop occurs in the electrolyte as indicated in the figure.

The leakage resistance can arise from different processes. One obvious reason is overcharging the capacitor with a voltage that is beyond the Faradaic oxidation or reduction potential of any constituent in the electrolyte. The most important source, however, is leakage through impurities, which are oxidized or reduced within the potential interval used in the capacitor; similarly, functional groups on the carbon surface can also contribute to leakage. If the impurity concentration is low, the self-discharge process will be diffusion-controlled, meaning that the limiting factor is the diffusion of reactant to the electrode surface. The kinetic reversibility of the Faradaic reaction determines the magnitude of R_F. Another route for the leakage is direct Ohmic leak. This can occur, for

example, if the electrode material percolates through the separator, forming a conduction path. [12, p. 483, pp. 560 – 561]

The leakage mechanism can be examined through measurement of the open-circuit voltage of a charged capacitor over a long time period. The rate-limiting step of the self-discharge process can be identified through the shape of the V versus time curve: linearity of V versus $\log t$ or versus $\sqrt{t}$, or of $\ln V$ versus t arise from activation-controlled Faradaic reactions, diffusion-limited reactions, and Ohmic leakage, respectively [23]. Another way of measuring leakage is through a float-current experiment, where the voltage is held constant by applying a small charging current matching the self-discharge rate [12, p. 562]. While the mechanisms of self-discharge are not as easily identified with this method, the leakage current is an important parameter from the applications point of view.

When a supercapacitor is charged, the electric potential of the positive electrode is higher than that of the negative electrode. The main potential drop is across the electric double layers (Fig. 2.3(b)). When charging or discharging the capacitor, there is also a potential drop across the bulk electrolyte. This is due to the resistance of the solution: ionic current flows through the capacitor when the electric double layer ions migrate to or away from the electrode. This potential drop is determined by the resistance of the solution, R_S, and the discharge current, I, by $V = IR_S$. The effect is illustrated in Fig. 2.3(b). The resistance may be higher across the separator than in other areas of the electrolyte, and is greater in organic solvents than in water. [12, p. 106]

Additional resistance is introduced with porous electrodes (see the next section). In practical devices, two different contact resistances can arise: between the particles of the active material, and between the active material and the current collector electrode. The resistance of the bulk electrode material, the current collectors and any outside leads also contribute to the measured device resistance. All the different resistances are usually grouped into one as the *equivalent series resistance* (ESR), which is a common parameter in traditional capacitor devices, depicting the dielectric losses seen in high frequencies. In supercapacitors, the ESR is an important figure of merit which limits the speed at which the capacitor can be charged or discharged, thus restricting the maximum power obtainable from the device. [12, p. 528]

2.1.3 Electrode porosity

The porosity of the electrode material has a significant effect on the properties of supercapacitors. The electrolyte resistance is largest for the ionic current going to the bottom of the pores, and smallest for the current going to the opening of the pores. This distributed resistance and capacitance can be described with a *transmission line model*, which is illustrated in Fig. 2.4 [24]. The effect of the distribution inside the pores is especially visible in alternate-current measurements, as it gives rise to a 45° impedance element (see Section 2.3.2) [12, pp. 378 – 379].

When the pores are very small, the diffuse layers of the EDL of electrode surfaces opposite each other may overlap, resulting in a very different distribution of ions. This effect is very strongly dependent on the ion concentration: the less concentrated the electrolyte is, the further the diffuse regions extend [12, p. 403]. In very small pores with diameters smaller than the size of the solvated ions, the double layer capacitance has been found to increase due to partial desolvation of the ions; this results in the ions moving closer to the surface [25]. A further complication with porous electrodes is surface wetting; the surface functional groups on the electrode affect the contact angle of the electrolyte [12,

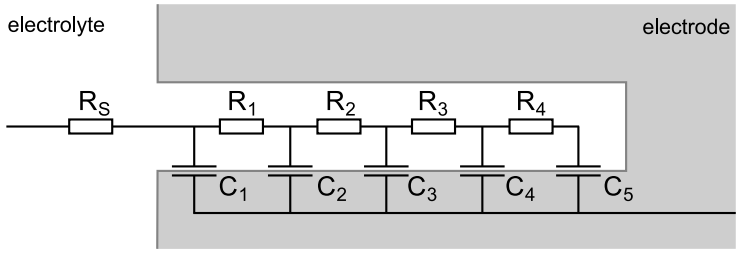

Figure 2.4: The distributed resistance and capacitance arising in porous electrodes.

p. 190]. Small pores may not be completely accessible to the electrolyte and thus cannot contribute to the capacitance.

When a supercapacitor is charged quickly, the whole surface of the porous electrode may not be covered evenly with charged ions; the surface near the pore openings is fully charged but the bottoms of the pores are not. In the circuit of Fig. 2.4 this corresponds to the leftmost capacitors being fully charged, and the rightmost charged only a little. After disconnecting the supercapacitor from the charging circuit, an internal *charge redistribution* takes place: ions move further down the pores, with the accompanying charge on the electrode following them. This corresponds, in Fig. 2.4, to the charge on all the capacitors evening out and reaching the same value. The result is an apparent decrease in the observed terminal voltage, which can be mistaken for leakage. [26]

2.2 Materials used in supercapacitors

Most commercial supercapacitor devices are based on activated carbon due to its low cost, high specific surface area and chemical stability. Extensive research has been directed at finding new alternatives to boost the specific energy and power, from specially designed porous carbons and carbon nanomaterials to pseudocapacitive metal oxides and conducting polymers. The electrolytes are divided into two basic categories: aqueous and non-aqueous. Most commercial supercapacitors rely on non-aqueous organic electrolytes, but aqueous ones are used as well.

2.2.1 Carbon

Activated carbon (AC) can be prepared by pyrolysis of biomass precursors such as wood, coal, coconut shells or peat. Today, practically all activated carbon used in supercapacitors is produced from coconut shells due to its price: supercapacitor-grade AC costs approximately $15/kg, which is very low compared to many other possible electrode materials. After pyrolysis, the resulting char is activated either chemically (e.g., treatment with potassium hydroxide) or physically (high-temperature treatment with an oxidizing gas). This opens up pores in the structure and removes disordered carbon material. Often, AC is blended with carbon black or graphite to improve the conductivity of the porous layer. [27–29]

Highly porous carbon materials, with carefully controlled pore size distribution and pore structure, can be prepared as carbon aerogels. They are obtained through pyrolysis of organic aerogels, the properties of which can be modified with processing conditions [29]. Carbon aerogels, as well as other polymer-derived carbon materials, are more conductive than AC, but their higher price currently prevents their use in commercial supercapacitors

[28]. Another precisely controllable way to produce porous carbon is from metal carbides such as titanium carbide [30]. The precursor is etched with chlorine gas, leaving behind a porous carbon structure. The process is, however, expensive compared to other methods [28].

Carbon nanomaterials, such as carbon nanotubes (CNT) and graphene, have attracted much attention in recent years. CNTs provide very good conductivity, but the active surface area is mostly limited to the outsides of the nanotubes; the "pores" of the material consist of the interstitial spaces between nanotubes [29]. Single-walled CNTs are currently too expensive for use in commercial applications, but multi-walled CNTs can be produced at approximately \$50/kg with similar performance to AC [28]. One challenge with CNTs is their low solubility, which results in difficulties with the processing. Additive dispersive agents are needed, but these then limit the performance of the electrodes.

Graphene, the one-atom-thick layer of sp^2-bonded carbon, is a promising material not only for supercapacitors but many other applications as well, including transistors, sensors and lithium-ion batteries [31]. Its good conductivity could enable high-power supercapacitor devices; it also has a high accessible surface area and good mechanical strength [32]. The structure of graphene materials is highly dependent on the preparation method – as is the cost of the produced material. For example, mechanical exfoliation of graphite, the method originally used to isolate graphene, leads to very high-quality graphene, but is not feasible in large-scale production [33]. Other methods include synthesis on silicon carbide, chemical vapour deposition, liquid-phase exfoliation of graphite and reduction of graphene oxide (GO). Of these, the last two are widely used in large-scale production. In liquid-phase exfoliation, intercalation of graphite by certain molecules, followed by, e.g., ultrasonication, leads to detached graphene sheets, although the yield is fairly low [33]. Graphene suffers from the same processing difficulties as CNTs in that additives are needed to keep the individual sheets from aggregating in solution.

Oxidation of graphite produces a material which has a high degree of defects because of a broken sp^2-bonded network, mainly with oxygen functionalities. This "graphite oxide" can then be dipersed in solution to yield GO. Reduction of GO can be performed chemically, thermally or electrochemically to partly restore the graphitic structure and its conductivity [33]. While the chemical method has been the most widely used, electrochemical reduction is a very attractive choice as it does not require the use of harsh chemicals [32]. In terms of price and performance, graphene materials could even be competetive with AC; however, the development is still ongoing [28].

2.2.2 Pseudocapacitive materials

Pseudocapacitance is a phenomenon in which charge is transferred across the double layer, as opposed to the electrostatic storage of energy in the purely double-layer capacitor. The mechanism of pseudocapacitance is Faradaic, but the reactions are fast, reversible, and take place at the surface of the electrode [30]. In reality, some chemical reactions do take place also at the surfaces of carbon electrodes, for example through oxygen-containing surface groups or impurities present in the device. The resulting pseudocapacitance can account for as much as 5 – 10% of the measured device capacitance [12, p. 188].

Pseudocapacitance can arise from a number of different mechanisms. One mechanism is potential-dependent electrodeposition, i.e. deposition of atoms on the electrode surface from solution through a Faradaic reaction. If the extent of oxidation/reduction of a metal oxide film depends on the potential, pseudocapacitance can arise. A common example

of this is RuO_2 on ruthenium surface, but the very high cost of the metal prohibits its practical use. Other transition metals with this property, such as manganese, have been extensively studied due to the lower cost. Another type of pseudocapacitance blurs the line between pseudocapacitive supercapacitors and batteries: intercalation of lithium ions into the electrode lattice. [34, pp. 221 – 222]

Pseudocapacitance is also observed with conducting polymers where the applied potential results in the charging of the polymer, doping it with anions (oxidized form) and cations (reduced form) [34, pp. 221 – 222]. The extent of oxidation or reduction depends on the potential, as with other types of pseudocapacitance. The most widely studied conducting polymers are polyaniline, polypyrrole and derivatives of polythiophene, the most popular of which is poly(3,4-ethylenedioxythiophene) (PEDOT) [35]. Supercapacitors based on conducting polymers exhibit good reversibility, but they usually suffer from poor cyclability due to volume changes during the reactions – which is a limitation in batteries as well. One solution to this has been to form composites with, for example, carbon nanomaterials, which improves the stability [35].

2.2.3 Electrolytes

There are two basic categories of electrolytes used in supercapacitors: aqueous and organic. Aqueous electrolytes perform better in terms of conductivity as well as cost, safety and ease of handling, but the electrochemical window (voltage window between oxidation and reduction of the solvent) is only 1.23 V [36]. The maximum voltage is very important, as the energy stored in a capacitor is proportional to the square of the voltage. Due to this, most commercial supercapacitor manufacturers use organic electrolytes, mainly acetonitrile and propylene carbonate, which can reach voltages of 2.5 – 3 V [30]. The most popular organic salts consist of lithium or tetra-alkylammonium ions as cations and tetrafluoroborate, perchlorate or hexafluorophosphate ions as anions [30, 37].

Stacking supercapacitor cells into modules is one way to increase the obtainable voltage with aqueous electrolytes and this has been used in commercial supercapacitor modules [37]. Common aqueous electrolytes are strong acids and bases, usually sulfuric acid or potassium hydroxide, due to their very high conductivity. Alkali salts such as KCl, NaCl and $NaSO_4$ have also been used due to the less corrosive nature of the neutral solutions [38]. One way to widen the electrochemical window of an aqueous electrolyte is to build an asymmetric supercapacitor from, for example, carbon and the pseudocapacitive manganese oxide. Such a configuration uses the hydrogen/oxygen gas evolution overpotential, which depends strongly on the electrode materials [39]. Aqueous $NaSO_4$ has been reported to enable 1.6 V or even 1.9 V voltages in symmetric carbon-carbon supercapacitors, with deaereated solvent and special pretreatment of the electrode materials [38, 40].

In recent years, ionic liquids have generated much interest as electrolytes. Ionic liquids are organic salts that have unusually low melting points, many of them liquid at room temperature. The low melting point is a result of at least one of the ions being large and unsymmetrical. The most important use of ionic liquids is in organic synthesis, where they are considered ‘green solvents’ due to their nonexistent vapour pressures and non-flammability. Ionic liquids are very stable, and being molten salts, conduct electricity well. Many ionic liquids, such as 1-ethyl-3-methylimidazolium bis(triluoromethylsulfate)imide (EMITFSI), have exceptionally wide electrochemical windows (as high as 4 V), making them attractive materials for supercapacitors. [41, 42]

Gel electrolytes are another interesting type of electrolyte to be used in supercapacitors.

Their solid-like structure removes the danger of electrolyte leakage, while the mobile ions enable conduction within the gel. A further advantage is that there is no need for a separator layer, since the gel itself functions as a separator. Common aqueous gel electrolytes are, for example, mixtures of poly(vinyl alcohol) (PVA) with potassium hydroxide or sulfuric acid [43, 44].

If a liquid electrolyte is used, a separator layer must be inserted between the electrodes to avoid short-circuiting the device. To ensure good ionic conductivity, the separator should be very porous and all eletrolyte constituents should be able to pass through it. Commonly, glassy fibrous separators, cellulose or filter paper are used.

2.3 Supercapacitor characterization

The three most common ways to characterize supercapacitors are cyclic voltammetry (CV), galvanostatic, i.e., constant current, charge-discharge (GCD) and impedance spectroscopy. CV is well suited to characterizing the properties of supercapacitor materials, especially in a 3-electrode setup. GCD is the recommended method for testing real device function, and impedance spectroscopy to study frequency dependence and transient processes in supercapacitors. [45]

Many parameters affect the measurement results, such as electrode thickness, current collector material and charging time before discharge. There have been intensive efforts to standardize supercapacitor measurements [45–47], but a single standard is yet to be adopted. Thus, when reporting properties, it is important to note the exact measurement conditions and procedures. [45, 48]

2.3.1 Cyclic voltammetry and galvanostatic charge-discharge

CV is a common method in electrochemical studies. A cyclovoltammogram is made by scanning the voltage linearly in time to a maximum value, and then scanning back to the original value, while recording the current. For an ideal capacitor, the shape of the curve is a rectangle; because $C = Q/V$ and $I = \mathrm{d}Q/\mathrm{d}t$, at constant $\mathrm{d}V/\mathrm{d}t$ the current is constant for a given sweep direction. In a real supercapacitor device, the curve is inflected due to resistance (Fig. 2.5a). There may also be an increase in current at the maximum-voltage end of the curve due to electrochemical reactions, such as those causing leakage.

There are different ways to calculate the capacitance from a CV curve. Basically, the capacitance is given by first integrating the current with respect to time to give charge, then dividing that by the potential interval. With a constant data sampling rate, this is equivalent to calculating the average current and dividing it by the voltage sweep rate. However, the choice of interval can have a significant effect on the result; different conventions are used, such as taking only the charging curve, or taking only the discharge from full cell to half-discharged. Additionally, the initial curve will give a different result from the curve after, e.g., 20 cycles. Either the discharge half of the curve or the whole curve are recommended to be used in calculations. [45, 48]

GCD is the recommended method for characterizing full devices and prototypes [45]. In this method, the supercapacitor is charged with a constant current while measuring the voltage; when the maximum voltage is reached, the current direction is changed and the supercapacitor discharged (Fig. 2.5b). The voltage can also be held at the maximum value for some time before discharge. In an ideal capacitor, the charge and discharge curves

are linear. This is also the case for most supercapacitors with little pseudocapacitive behaviour, as well as many pseudocapacitors [45].

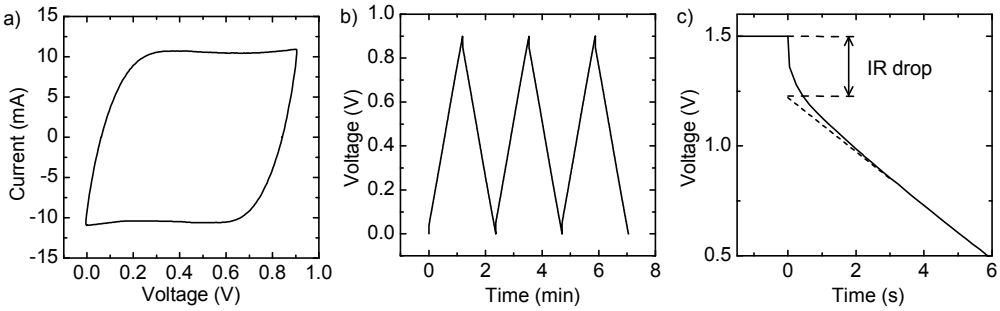

Figure 2.5: Examples of supercapacitor measurements: a) CV curve, b) galvanostatic charge-discharge, and c) galvanostatic discharge after voltage hold with extrapolation to find the correct IR drop value.

In the beginning of the discharge, there is a drop in voltage due to the ESR of the device, corresponding to $V = R\Delta I$, where ΔI is the change in current. The ESR can then be calculated from this voltage drop. If the current is zero before the discharge, ΔI is the discharge current; if there is a quick switch from charging at I to dicharging at I, the change in current is $\Delta I = 2I$ [45]. However, in supercapacitors there is usually an additional, more gradual voltage drop after the initial one (Fig. 2.5c) due to the slower response of the electrolyte in the pores of the device. Because of this, it is recommended that the straight part of the discharge curve is extrapolated to the beginning point of the discharge, and that value used for calculation [46]. The extrapolated IR drop value can be up to twice that of the instantaneous one [47].

The capacitance is calculated from the discharge curve as:

$$C = I \times \frac{t_2 - t_1}{V_2 - V_1}\,, \tag{2.2}$$

between points 1 and 2 on the discharge curve, or by linear fit of the data in this interval. In the IEC standard [46], these points are where the capacitor voltage is 80% and 40% of the fully charged device. The capacitance can also be calculated from the whole curve after the IR drop, which yields the same result when the curve is linear [45]. The choice of discharge current affects the results of GCD. In general, increasing the current results in the decrease of both capacitance and ESR [45]. In the IEC standard, the current is defined with regard to the capacitance in four application classes [46].

2.3.2 Impedance spectroscopy

Impedance spectroscopy is a versatile tool for characterizing many transient processes in electrochemical systems [49]. The method consists of applying a small (5 – 10 mV) alternating voltage $v(t)$ and measuring the resulting alternating current $i(t)$, optionally on top of a DC offset voltage. The voltage and current are related by

$$v(t) = \bar{Z} i(t) \quad , \tag{2.3}$$

where $\bar{Z}$ is the complex impedance. It can be represented as a magnitude and phase angle ($|\bar{Z}|$ and ϕ), or as real and imaginary components (Z' and Z''). The measurement

frequency is swept from about 1 mHz to 1 MHz [49], resulting in a spectrum of impedance data. The real part of the impedance is related to the device resistance: sometimes, the value of Z' at 1 kHz is taken as the ESR [47]. This value can, however, be significantly lower than that measured with the galvanostatic method [47].

An example impedance curve, plotted as Z'' versus Z' (a *Nyquist plot*), is shown in Fig. 2.6. The values of Z'' are negative for a capacitor, so the plot is usually drawn with a negative vertical axis. As both axes are in units of Ω, the axis spacing should be the same. At low frequency, the plot tends toward a vertical line, which is characteristic of an ideal capacitor. The shift in the Z' direction is indicative of a series resistance.

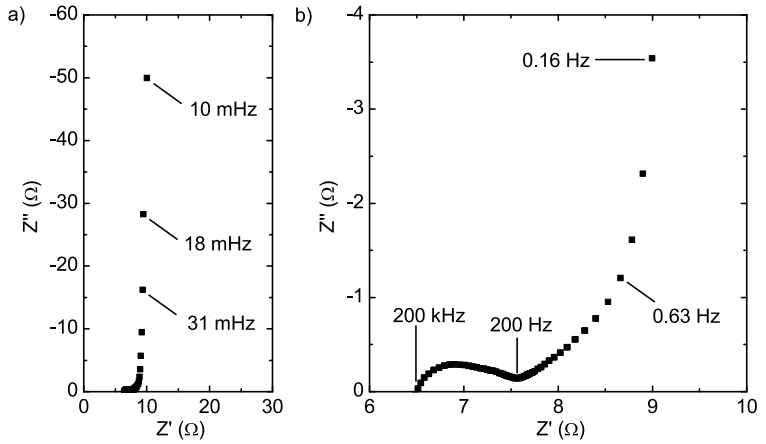

Figure 2.6: Example of a Nyquist plot of impedance data; b is a close-up view of a.

At medium frequencies, there is a section of the Nyquist plot with approximately 45° angle. This arises due to the transmission line behaviour (Section 2.1.3) of the porous electrode material [34, p. 484]. The width of this area depends on the electrode thickness [50]. At the highest frequencies, a semicircle is often observed in supercapacitor measurements. The cause is a parallel RC-element in the system [12, p. 494]. It has been shown by Portet et al. that the most likely reason is an imperfect electrical contact between the current collector and the active material: the contact interface effectively contains a resistance and an interface capacitance in parallel [51]. In reality, the semicircle is rarely a perfect one with its center on the real axis: different distributed elements and processes with different relaxation times can distort the shape of the curve [49].

The impedance data can be used to calculate a complex capacitance, $\bar{C} = C' + iC''$ according to [50]

$$C' = -\frac{Z''}{2\pi f|\bar{Z}|^2} \quad \text{and} \quad C'' = \frac{Z'}{2\pi f|\bar{Z}|^2} \,. \tag{2.4}$$

The real part, C', is related to the device capacitance and its value at the lowest frequencies corresponds to the galvanostatically measured capacitance. The imaginary part, C'', is related to resistive losses in the device. Plotted against the frequency, C'' goes through a maximum at some frequency f_0; the reciprocal of this frequency is a characteristic time, τ_0, which describes how quickly the supercapacitor can be charged and discharged with over 50% efficiency [25].

2.3.3 Energy and power

The energy stored in a capacitor is calculated from

$$E = \frac{1}{2} C V_{max}^2 \quad , \tag{2.5}$$

where V is the maximum voltage. The formula applies to supercapacitors as well, when the GCD is linear [45]. However, in most applications energy drawn from the supercapacitor is only useful if the voltage is over, e.g., $0.5 V_{max}$ [47, 48]. In this case, only 75% of the stored energy can be used, and the formula becomes [47]

$$E = \frac{3}{8} C V_{max}^2 \, . \tag{2.6}$$

This is still a simplified form, as a full description of the energy capability requires the relationship between power and energy: the usable energy usually decreases with increasing power [47]. The energy is commonly reported normalized to the mass or volume of the device or the active material; the values in commercial supercapacitors range from 1 to 6 Wh/kg for full devices. Taking into account only the active mass (e.g., the activated carbon in the device), 15 to 25 Wh/kg is obtained. [45]

The maximum power that can be drawn from a supercapacitor occurs when the load resistance is equal to the ESR (match impedance). In this case, the power is

$$P_{max} = \frac{V_{max}^2}{4 \times \mathrm{ESR}} \, . \tag{2.7}$$

This is the value most often reported, but the usable power in real applications is closer to half of P_{max}. In a pulse power measurement, only approximately 1/10 of P_{max} is available. Specific power values for commercial supercapacitors range from 2 to 20 kW/kg for full devices and from 20 to 120 kW/kg for only the active material. [45]

2.3.4 Other factors affecting supercapacitor performance

The leakage pathways described in Sec. 2.1.2 result in an eventual discharge of the supercapacitor, and thus the magnitude of leakage is an important parameter to measure. There are two basic ways for leakage determination: a float current method, and a self-discharge method [23].

In the float current method, the supercapacitor is charged to the maximum voltage and held there for a period of time, ranging from 1 hour to 72 hours, to ensure that the electrode surface is charged evenly [45, 46]. Due to leakage, a small float current is needed to maintain the voltage – this current is then recorded as the leakage current of the device, after a specified time [45, 46]. In the self-discharge method, the supercapacitor is fully charged, again holding the maximum voltage for some hours to ensure full charging [45, 46]. After this, the device is disconnected and its voltage monitored over time. For continuous measurement, the voltmeter used should have a very large input impedance. Alternatively, the voltage can only be measured at certain intervals and the supercapacitor disconnected between measurements. The two leakage current measurement methods are not equivalent: the reactions causing leakage depend on voltage, so that at a higher voltage more reactions occur. In the self-discharge test, the declining voltage affects which leakage processes can take place.

The cycling stability of supercapacitors is also closely related to the electrochemical processes occuring in the device, because they are the main cause of device degradation; an ideal electrostatic supercapacitor would have very little degradation. The majority of these processes occur near the maximum operating voltage, and thus the choice of maximum voltage is an important one to the device stability. For example, in practical supercapacitor module systems, where several cells are connected in series to achieve a higher voltage, each cell is operated approximately 10% below the rated voltage, to ensure a longer lifetime [52]. Due to added pseudocapacitive contributions, a higher voltage usually results in a higher capacitance value. Because of this, and the larger energy, there is a clear trade-off in the choice of maximum voltage, between the performance and the stability of the supercapacitors.

Commonly, cycling stability is tested through charge-discharge cycles with constant current, which is very time-consuming. Moreover, Weingarth et al. note that in such a cycling test, the voltage of the supercapacitor is well below values where most degradation processes occur, for most of the test duration [53]. They propose instead a hold test, where the supercapacitor voltage is held at a maximum for several hours at a time, measuring device properties at regular intervals. This results is a faster degradation and thus a quicker, more reliable test of device properties [53].

The test setup used can have a significant impact on the results of supercapacitor measurements. The mass, thickness and packing density of the electrodes is an important example: a very small amount of material can lead to higher capacitance and lower resistance than would be observed in a real application [48]. Stoller and Ruoff recommend to use at least 10 mg active material mass in laboratory tests [48]. There are also many inconsistencies in reporting specific values, which can be given in relation to mass, volume, or footprint area. Some reports only use the active material mass, others the mass of the active electrode including binder and other additives, and some the whole cell with electrolyte, current collectors and packaging [45]. Sometimes, the tests are carried out by simply immersing the electrodes in a beaker glass with electrolyte; this approach will dilute impurities in the electrodes to such extent that true effects on leakage current and cyclability cannot be observed [28].

The apparent performance of supercapacitors depends on the measurement rate: either the CV voltage sweep rate or the current used in GCD [45]. It is therefore very important to disclose the rate used in the measurements. Many reports include rate dependence data, i.e., the capacitance measured at different discharge currents or CV curves at different sweep rates. When using very low charge/discharge rates, especially combined with small amounts of material, the leakage current in the device can become comparable to the measurement current, which affects the results [48]. Temperature is another factor with significant effects on the capacitance and, in particular, the ESR, and should be taken into account as well. The ESR generally increases with decreasing temperature as the resistance of the electrolyte increases; due to the ESR increase, the capacitance decreases with decreasing temperature when measured at high frequency or discharge rate [54].

Increasing the voltage hold time before galvanostatic discharge affects the measured ESR significantly. [45]. With no voltage hold, the obtained ESR is very low, but it increases with the hold time up to 30 minutes [45]. This is due to the charge redistribution in the porous electrode layers; the longer time allows for the bottoms of the pores to be charged fully, which also increases the resistance when those areas are discharged.

2.4 Printed supercapacitors

Supercapacitors are commonly prepared similarly to batteries, rolling electrode layers and separator between current collector films and packaging the device in rigid metal or plastic casing [55]. Supercapacitors can, however, be prepared through printing on plastic substrates, facilitating the possibility of flexible devices [15–18, 56].

Most reports on printed supercapacitors describe devices in which the electrodes are printed on separate substrates and sandwiched together with a separator paper to form the device [13, 16, 18, 57, 58]. There have also been demonstrations of using gel electrolytes, which enables leaving out the separator layer [15, 18, 59, 60]. Printing all the layers on the same substrate has been reported [59], although the fundamental problem in monolithic printing is the separator layer: it should not be permeable to the ink used to print the top electrode, but should still allow electrolyte to move through it as freely as possible. Hu et al. have demonstrated using the separator as the substrate, with electrodes printed on both sides [61]; in this case as well, there is a need for blocking polymer layers on the separator to prevent ink from penetrating the paper, which then increases the ESR of the device.

The main requirement for choosing the printing method is the thickness of the film; compared to most printed electronics devices, fairly thick films of the active material (on the order of tens of micrometers) are needed in supercapacitors. On the other hand, the print image resolution is not critical. Screen printing is a good choice for producing thick, patterned electrodes, and it has been used in many studies [16, 57, 58, 62]. In screen printing, a viscous, shear-thinning ink is forced through a polyester screen by a rubber squeegee (Fig. 2.7a). The screen is patterned by blocking the mesh in areas outside the print image.

Simpler methods for depositing thick layers are doctor-blade coating and rod-coating [13]. In the doctor-blade method, the ink is simply spread with a sharp blade held at a specified distance from the substrate (Fig. 2.7b). Patterning of the printed electrode can be done with a stencil mask. In rod-coating, a wound-wire-patterned rod is used to spread the ink; the resulting layer thickness depends on the spacing and thickness of the wires. The advantage of these methods is their simplicity: electrodes can be prepared manually for quick testing. Other methods used for printable supercapacitor electrode fabrication are dispenser printing [59, 60], spray-coating [15] and flexographic printing [18].

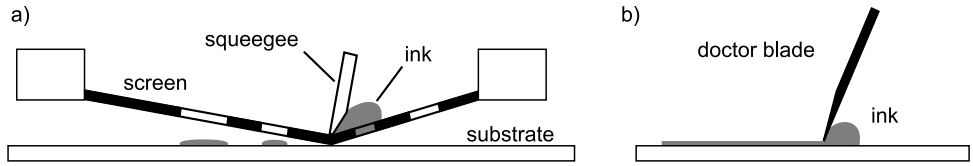

Figure 2.7: Schematic drawings of a) the screen printing process and b) the doctor blade method.

Inkjet printing, which can be used to produce small features in thin layers, has also been utilized in supercapacitor fabrication. With inkjet, the two electrodes can be patterned on the same substrate in an interdigitated finger configuration to form a *micro-supercapacitor*; usually, metal deposition and etching has been used for the patterning. A solid or gel electrolyte is deposited on top of the structure. Micro-supercapacitors usually have

Table 2.1: Results of printed or coated activated carbon supercapacitors in the literature. The specific capcitances are calculated from the device capacitance and the entire active mass.

printing method	area (cm^2)	C/area (mF/cm^2)	C/m (F/g)	ESR × area (Ωcm^2)	electrolyte	V_{max} (V)	Ref.
dispenser	37.5	10–40	–	–	organic	2.5	[60]
bar-coating	2.0	50–250	30–35	0.72–6	aqueous	1.2	[13]
screen	4–6	190–510	63–88	14–50	aqueous gel	1.0	[58]
screen	56	44–173	–	300–13000	ionic liquid	1.5	[16]
flexographic	25	0.72–4	–	31–99	aqueous gel	0.8	[18]

capacitances on the order of 1 mF/cm^2 and they can be utilized, for example, as small on-chip energy storages in ubiquitous electronics. [63, 64]

Literature reports of printed supercapacitors based on AC are summarized in Table 2.1. Comparison of such devices is often challenging due to differences in measurement setups, procedures and calculations [65]. The thickness of the active layer is the most important factor determining the capacitance of the device: it is possible to reach up to $0.5\,F/cm^2$ with very thick AC layers of $6–12\,mg/cm^2$ [58]. The electrolyte and applied voltage range also affect the capacitance. Novel materials, such as carbon nanomaterials, pseudocapacitive oxides, or composites of the two have also been used in printed supercapacitors. Table 2.2 summarizes results from selected publications; there are large variations in the specific capacitance values but they are for the most part larger than those of the AC supercapacitors.

2.5 Energy harvesting

In recent years, there has been a growth in portable, wearable and distributed electronics such as sensors. Energy harvesting has been proposed as the most suitable energy source for such applications; replaceable or even rechargable batteries are in many cases not feasible due to the large number of distributed devices, and due to the toxic chemicals present in batteries. Harvesting energy from ambient sources enables placing wireless sensors and other devices in places that are difficult to reach, such as in remote geographical areas, inside building structures, or implanted in human bodies. Large numbers of devices can be deployed without the need for maintenance or battery change. [1, 2, 69, 70]

Energy can be harvested from motion, temperature differences, light, radio frequency (RF) waves, or biochemical sources. Motion or vibration can be captured with the use of electrostatic, electromagnetic, or piezoelectric harvesters; thermal energy can be harvested with thermocouples based on conductor juctions; RF energy can be gathered with antennas; microbial fuel cells can convert chemical energy in biodegradable materials to electrical energy. Light is the most widely used source, also utilized in grid-scale energy production, and its power output in outdoor settings is the highest one of the harvesting methods. [1, 71]

The output of an energy harvester can rarely be used to directly power an electronic device; in practice, control circuitry is needed to, e.g., convert AC to DC or the opposite, or to increase the voltage with a charge pump. Moreover, an interim energy storage is needed, because the device may need large power peaks and low power in between them,

Table 2.2: Results in the literature on printed or coated supercapacitors with pseudocapacitive materials, composites, and nanomaterials. The specific capacitances are calculated for the entire device, except where noted otherwise.

material	printing method	C/m (F/g)	electrolyte	V_{max} (V)	Ref.
RuO_2 nanoparticles / PEDOT:PSS / graphene	screen	820[1]	H_2SO_4	0.8	[62]
asymmetric $LiCoO_2$ and graphene oxide	screen	58	organic	1.5	[57]
MnO_2-coated carbon microspheres	screen	– (19 mF/cm^2)	aqueous gel	0.8	[66]
CNT	inkjet	33	organic	3.0	[61]
CNT	spray-coated	90–120[2]	aqueous gel	1.0	[15]
CNT	inkjet	235	ionic liquid gel	3.0	[67]
graphene (interdigitated)	inkjet	– (0.1 mF/cm^2)	aqueous gel	1.0	[64]
reduced GO	inkjet	124[3] 192[3] 73[3]	K_2SO_4 H_2SO_4 ionic liquid	1.0 1.0 3.0	[68]

[1] 3-electrode measurement of one electrode; result 4 times larger than with a 2-electrode device

[2] value calculated from device capacitance and the mass of only one electrode

[3] 2-electrode device measured, results multiplied by 4, corresponding to 3-electrode measurement

such as when a wireless sensor intermittently transmits data, and the primary energy source may not always be available. In the case of long-term operation, the cyclability of the energy storage unit becomes the most important requirement, making supercapacitors a superior alternative to batteries. [2, 69]

Another application of energy harvesting where supercapacitors are useful is regenerative braking in vehicles, where the peak power of collected energy is too large to use for battery recharging directly. In some applications, a combination of a supercapacitor and a battery is the best option, to utilize quick charge and discharge power through the supercapacitor, and the large energy capacity of the battery. [19]

3 Materials and methods

In this chapter, the sample preparation and characterization is is described briefly. More detailed descriptions of the experiments are given in the publications **I**–**IV**. The substrate material in all samples was poly(ethylene terephtalate) (PET), which has very good surface properties in terms of printing, as well as good heat stability.

3.1 Electrodes

The current collectors in **I** and **III** were prepared by first evaporating a copper or silver layer on the substrate, then blade-coating a layer of conducting graphite ink (Henkel/Acheson Electrodag PF407C) on top of the metal. The graphite layer protects the metal layer from corrosion. In **IV**, only the graphite ink was used as current collector: two layers were printed with a semiautomatic screen printer.

Two commercially available activated carbons were used in this work as active layer: Norit DLC Super 50 [**I**], and Kuraray YP-80F [**IV**]. The former has a specific surface area of approximately 2000 m^2/g and the latter 2100 m^2/g according to the supplier. The ACs were formulated into inks using carboxymethyl cellulose as binder with Norit and shrimp-shell derived chitosan with Kuraray, both at approximately 5% of the ink dry mass. The solvent for the ink was water, which facilitates a very simple ink handling and cleanup, but which evaporates very quickly compared to typical screen printing solvents.

The Norit ink was blade-coated on the current collector, which enables using only small amounts of ink at a time and carrying out the coating before the ink dries. The Kuraray ink was screen printed; during the print, deionized water was sprayed on the screen intermittently to prevent the ink from drying on the screen. This, however, resulted in some variation of the printed layer thicknesses, as the ink was alternately concentrated through water evaporation and diluted through the addition of water [**IV**].

A carbon nanotube (CNT) ink was obtained from Morphona Ltd (Finland). The ink is an aqueous dispersion of multi-walled CNTs in water with a xylan hemicellulose polymer as a dispersant/binder. The polymer constituted approximately a third of the ink dry mass; the large amount is needed to disperse the nanotubes, which otherwise tend to aggregate. The ink was blade-coated into 1.4 cm wide electrodes, using multiple coating passes to achieve a sufficiently conducting layer. The ink functioned as both the current collector and active material, so other layers were not needed. [**II**]

PEDOT and and its composites with graphene oxide (GO) were prepared at the University of Turku on metal/graphite current collectors. PEDOT was prepared through electropolymerization of 3,4-ethylenedioxythiophene in an ionic liquid; adding dispersed GO in the solution resulted in the negatively charged GO flakes being embedded into the polymer layer as counterions. Electrochemical reduction was used to convert the GO to

reduced graphene oxide (rGO). The charge consumed by the polymerization was kept constant in all samples, so that layers with similar PEDOT content were produced. Both potentiostatic and cyclic voltammetry electropolymerization methods were tested, and the CV method found to produce better layers. [**III**]

3.2 Device fabrication

The supercapacitors were assembled from two similar electrodes and a separator paper, which were sandwiched together. The electrodes and separator were saturated with aqueous LiCl (**I**) or NaCl (**II**–**IV**) before assembly, and the lamination of the layers done by carefully rolling the top electrode on the bottom one in such a way that the amount of air trapped in the device was minimized. In **I**–**III**, the electrodes were placed in a 90° angle with respect to each other with the square-shaped active areas overlapping. The electrodes were 1.4 cm or 2.0 cm wide, yielding 2 and 4 cm^2 active areas, respectively. In **IV**, the electrodes were wider (2.0 cm) and shorter, and the assembly done with a head-on configuration; the active area was 1.8 cm wide and 1.0 cm long.

The substrates were sealed together with an adhesive film (in **I**–**III**), which was cut as a square gasket and placed around the active area. In **IV**, heat-sealing was used; as PET itself could not be heat-sealed, an ethylene-copolymer dispersion in water (Paramelt Aquaseal) was applied on the edges of the substrate, dried, and the device edges heat-sealed.

3.3 Characterization

Cyclic voltammetry (CV) and galvanostatic charge-discharge (GCD) were performed with a Zahner Zennium potentiostat (**I**–**III**) or a Maccor 4300 battery test system (**IV**). The IEC standard [46] was used as a basis for the characterization: the capacitances were derived from the discharge curve at constant current after a 30-minute voltage hold, except for **I** where a 5-minute hold was used. The maximum voltage was 0.9 V for all measurements. Additionally, a voltage test was performed with the screen printed supercapacitors to examine the effect of the maximum voltage (from 0.8 V to 1.2 V) on the device properties.

The ESR was calculated from the IR drop of a GCD curve with 10 times higher current than that used for the capacitance measurement [46]. A linear fit was made to the discharge curve between 1% and 20% of the discharge time; the fit at this interval was visually estimated to best correspond to the fitting procedure described in [46]. The leakage current was recorded after 30 min or 1 h hold at the maximum voltage.

In the measurements performed on the Maccor system (**IV**), a long measurement program could be used, covering three charge-discharge cycles, a 30-minute voltage hold and discharge for capacitance/ESR determination, and a 1-hour voltage hold for leakage current determination. These steps were repeated three times for three different currents (here, 1 mA, 3 mA and 10 mA), after which CV curves were measured at 100 mV/s, 50 mV/s, 10 mV/s and 5 mV/s, four cycles for each. In **IV**, discharge at 1 mA was used for capacitance calculation and discharge at 10 mA used for ESR calculation. The reported leakage current was taken from the end of the third 1-hour segment. The measurement is illustrated in Fig. 3.1.

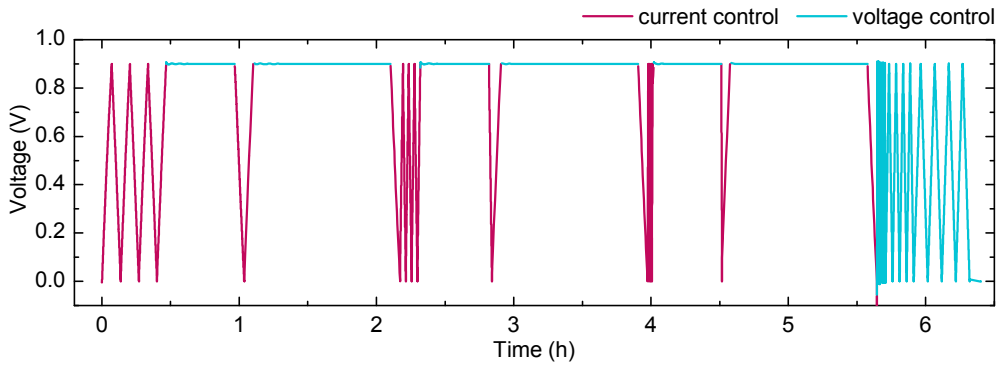

Figure 3.1: The measurement program used in **IV**. The voltage-controlled part in the end is the CV measurement.

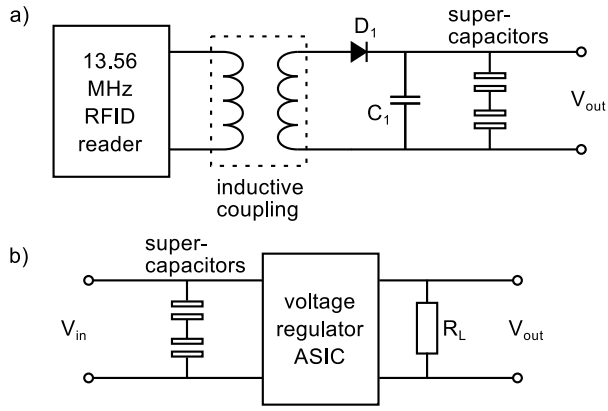

Figure 3.2: Schematics of the harvester a) charging circuit and b) operation circuit. Adapted from **I**.

Impedance spectrocopy was performed with the Zahner Zennium potentiostat in the frequency range from 10 mHz to 1 MHz. An amplitude of 5 mV and offset of 0 V were used. The samples were discharged well by short circuiting prior to the measurement.

3.4 Energy harvesting

The metal/graphite AC supercapacitors were used in an energy harvesting demonstration with a printed RF harvester. A circuit diagram of the experiment setup is shown in Fig. 3.2. An RFID reader was used for charging the supercapacitor through a printed antenna and rectifier; two reader – antenna distances were used to give the rectifier either a high or a low input signal amplitude. Two similar supercapacitors were connected in series to reach a higher voltage; two different device sizes were tested. [**I**]

The supercapacitor operation after RF harvesting was then demonstrated with an application-specific integrated circuit (ASIC), which gives a steady output of 1.2 V, suitable for powering, e.g., a small sensor. A 1 MΩ load (R_L) was connected to the ASIC output and the voltages of the supercapacitors and the output monitored through probes

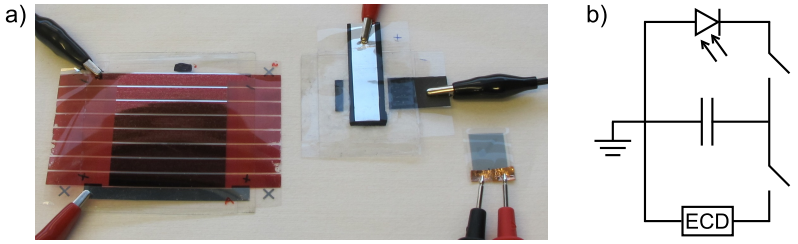

Figure 3.3: a) A photograph and b) a circuit schematic of the OPV/ECD harvester setup. Adapted from **III**.

with high input impedance. [**I**]

A PEDOT/rGO supercapacitor was used in another energy harvesting demonstration; here, a gravure-printed organic photovoltaic (OPV) module, provided by VTT (Oulu, Finland) [72], was used to charge the supercapacitor in ambient indoor lighting (Fig. 3.3). After charging, the supercapacitor was disconnected from the OPV module and used to switch a small electrochromic display (ECD), provided by Acreo (Sweden), on and off repeatedly by reversing the lead contacts every two seconds. [**III**]

4 Results and discussion

4.1 Activated carbon supercapacitors

The supercapacitors were assembled in two different configurations: 90° angle [**I**] and head-on [**IV**]. The 90° angle enabled simpler assembly, because the square-shaped active layers could be easily aligned. This approach worked well in supercapacitors with a metallic current collector under the graphite one, as the different total resistance from the external contact to different sides of the active area was low. In supercapacitors with only graphite current collectors, the electrode configuration needed to be optimized: the electrodes were made wider and shorter, and the assembly done with a head-on configuration. The device structures are presented in Fig. 4.1.

The capacitance and ESR results of the AC supercapacitors are presented in Table 4.1. As the AC mass loading was larger in the supercapacitors with only graphite as current collector, the areal capacitance is larger. The electrolyte (LiCl vs. NaCl) and the activated carbon were also different, which may affect results. The smaller capacitance of the $2\,\mathrm{cm}^2$ supercapacitors compared to the otherwise similar $4\,\mathrm{cm}^2$ devices with metal current collectors may be due to slight inaccuracies in depositing and weighing the AC ink.

In the metal-graphite-AC supercapacitors, there is considerable difference between the ESRs of the devices despite the highly conductive metal layer. When the current collectors are narrower, as was the case here, the contact area between the metal and graphite is also smaller, which can increase the interfacial resistance between the two layers. Overall, it can be concluded that similar performance can be reached with only graphite as the current collector material. This is an advantage in terms of device reliability, as the copper layer will be corroded if there is a defect in the overlaying graphite layer and the electrolyte comes into contact with it.

The large number of supercapacitors prepared by screen printing in **IV** revealed significant variation between samples. The manual adjustment of the squeegee pressure and other

Table 4.1: Results for activated carbon supercapacitors, calculated from galvanostatic discharge after a voltage hold. An average value is shown for the devices reported in **IV**.

active area size	current collector	AC loading ($\mathrm{mg/cm^2}$)	C/area ($\mathrm{mF/cm^2}$)	ESR (Ω)	Ref.
$2\,\mathrm{cm} \times 2\,\mathrm{cm}$	metal + graphite	2.2	110	4	**I**
$1.4\,\mathrm{cm} \times 1.4\,\mathrm{cm}$	metal + graphite	2.2	100	10	**I**
$1\,\mathrm{cm} \times 1.8\,\mathrm{cm}$	graphite	3.7	150	10	**IV**

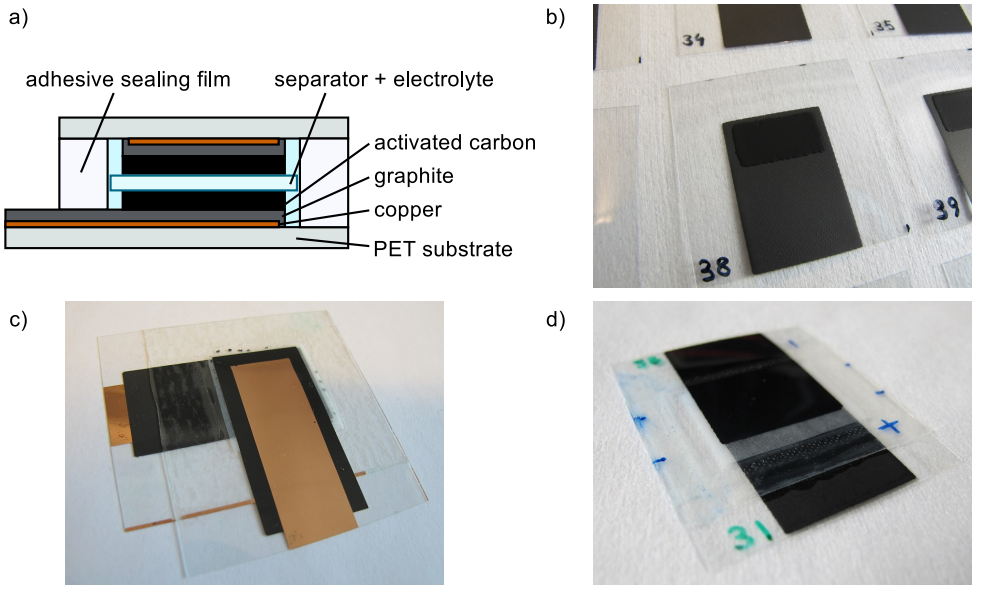

Figure 4.1: a) Schematic of the supercapacitor assembly. The copper layer was used in **I** but not in **IV**. b) Printed electrodes on graphite current collectors. c) A supercapacitor sample with metal and graphite current collectors, assembled in 90° angle. d) A supercapacitor with only graphite current collectors, assembled with head-on conguration. Figures a and c adapted from **I**, b and d from **IV**.

parameters – such as screen height and squeegee speed – resulted in different layer thicknesses produced on different fabrication times. The differences could have been avoided by printing many more samples than needed, measuring, e.g., the sheet resistances of the graphite, and selecting only the ones with similar resistance to be used in devices. However, the use of different electrodes, both in terms of graphite layer conductivity and AC layer mass loading, enables examination of the dependence between the parameters as well as optimization of the devices.

The correlation between capacitance and AC mass is not very good (Fig. 4.2a), despite the straightforward theoretical correspondence between the two. One possible cause is inaccuracy in weighing the AC layer; the small amount of material added on a relatively large sheet of plastic is difficult to weigh reliably. Another is the amount of AC material which is actually taking part in the charge storage: poor contact to the current collector or incomplete access of the electrolyte can render the AC material inactive. The former was investigated in **IV** through a pressing test, where the AC layers were pressed after printing to ensure good contact between the particles, similarly to the fabrication of pressed active material pellets in many studies on new supercapacitor materials. However, no difference was found to the samples with unpressed electrodes.

The specific capacitance, calculated from the total AC ink dry mass including binder, ranged from 16 F/g to 26 F/g. It decreased with increasing AC mass, even though the mass was on the order of that recommended by Stoller and Ruoff [48]. The dependence should be taken into account when designing devices of a given capacitance for applications. The average value, 20 F/g, corresponds to the single-electrode value of 80 F/g, which is much lower than the highest reported literature values for activated carbon (up to

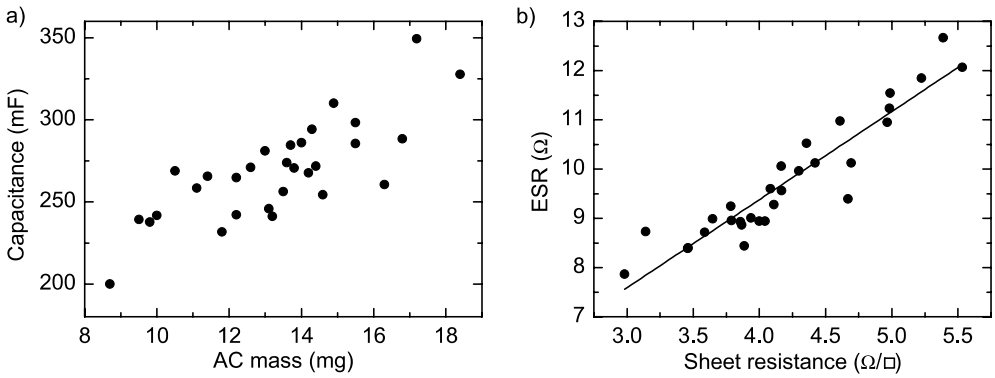

Figure 4.2: Results for screen printed AC supercapacitors with NaCl electrolyte, measured with galvanostatic discharge from 0.9 V. a) Capacitance plotted against the total activated carbon ink mass in the supercapacitor. b) Supercapacitor ESR plotted against the average sheet resistance of the two electrodes in the device, with a linear least-squares fit. Adapted from **IV**.

200 F/g [30]). However, such high values are typically obtained in optimized test setups and single-electrode measurements; the results for the full devices are expected to be lower, e.g., due to the different capacitance of the same material in positive and negative electrodes (Sec. 2.1.1).

Previous literature on printed supercapacitors with a symmetric 2-electrode configuration have reported specific capacitances from 30 to 88 F/g (Sec. 2.4). Keskinen et al. [13] calculated the value from only the activated carbon content in the device, not including the binder, which explains some of the difference; a higher voltage was also used, which increases the capacitance (Sec. 4.3.2). The very high specific capacitance of 88 F/g obtained by Jost et al. [58] may be in part due to the fabric current collector, which allows the AC to be deposited around the fibers, ensuring good electrical pathways to the current collector from the active areas, essentially reducing the active layer thickness.

In printed supercapacitors, a more interesting figure of merit than the specific capacitance is the areal capacitance; the specific capacitance is for the most part a property of the active material. The areal capacitance reveals the capacitances which can be obtained in actual printed devices. The most important parameter is the printing method, which determines the obtainable layer thickness. Most reports in literature utilize screen or dispenser printing, which have yielded capacitances ranging from 10 to 510 mF/cm^2 [13, 16, 58, 60]. The best areal capacitance obtained here, 150 mF/cm^2, is in the middle of the range. The relatively low values reported by Somov et al. (10–40 mF/cm^2) [60] and Pettersson et al. (44–173 mF/cm^2) [16] may be related to the organic and ionic liquid electrolytes containing large ions, which may not fit the pores of the active material as well as aqueous electrolyte ions. The larger areal capacitances obtained by Keskinen et al. [13] and Jost et al. [58], both of which utilize aqueous electrolytes, are explained by the same factors as for specific capacitance. In particular, the fabric current collector in [58] enables a very large mass loading of the active material to be used in the device. However, the final device in that case must be sealed in additional plastic casing outside the fabric to prevent skin contact to the acidic gel.

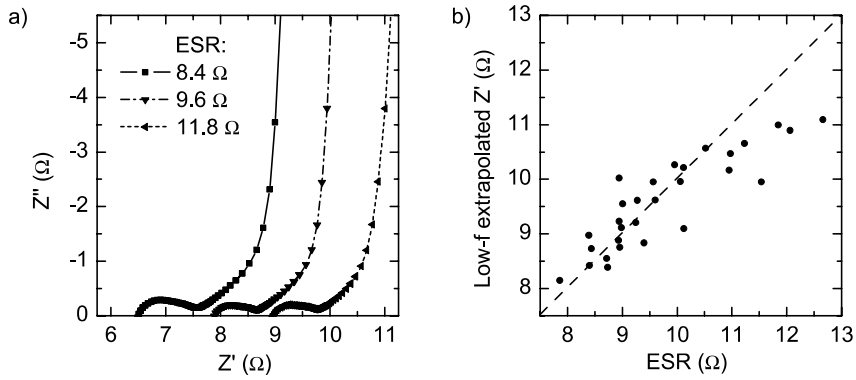

Figure 4.3: a) Nyquist plots of three AC supercapacitor samples and b) their intersection of the Z' axis when extrapolated from the low-frequency values (dashed line indicates the same resistance value). Adapted from **IV**.

4.1.1 Resistance

Fig. 4.2b shows the dependence of the device ESR on the average sheet resistance of the graphite electrodes for 30 supercapacitor samples using NaCl electrolyte. The correlation between the two is fairly good: the adjusted r^2-value (coefficient of determination) of a linear fit is 0.87. The vertical axis intercept of the fitted line is 2.2 Ω. This value can be interpreted as the average contribution to the ESR by parts other than the current collector layer; the main sources are the resistance of the activated carbon layer and its contact with the current collector, as well as the resistance of the electrolyte. The distributed resistance in the pores of the active material is another important cause of resistance.

The resistances can be more closely examined through impedance spectroscopy; examples of the impedance plots are shown in Fig. 4.3a. It is easily seen that the galvanostatically measured ESR corresponds to a shift in the position of the curve along the real axis, the semicircle left end position ranging from 6 to 9 Ω. Taking the lowest-frequency points (below 0.2 Hz) and extrapolating a fitted line to the real axis results in a resistance value which should correspond to the ESR. The extrapolated values are shown in Fig. 4.3b plotted against the ESR, and indeed, there is some correlation. However, at ESR values over 11 Ω the value extracted from the Nyquist plot is lower. Possibly, the frequency at which the device begins to resemble truly capacitive behaviour is shifted to even lower frequencies when the resistance is large, and thus the fit should be done at lower frequencies too. [**IV**]

The 45° section of the Nyquist plots originates from the distributed resistance and capacitance of the porous electrode. Its width (0.8 – 1.5 Ω) was found to approximately correspond to the device capacitance, which supports the notion that the source is in the active layer, the cumulated resistance being larger the more active material there is [**IV**]. The semicircle obtained at high frequencies is caused by the contact resistance and capacitance between the active material and the current collector, as outlined in Sec. 2.3.2, and its width (0.5 – 1.1 Ω) corresponds to the value of the contact resistance. The flattened shape of the semicircle indicates, however, that there may be more complex processes involved; the interpretation is thus only an approximation. The total resistance of the screen-printed supercapacitors can then be assigned to the constituents as summarized in

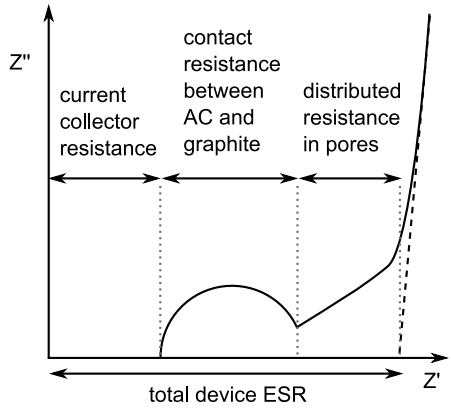

Figure 4.4: Summary of the components making up the ESR, as observed in an impedance spectroscopy experiment.

Fig. 4.4.

This analysis can be used to optimize supercapacitor performance: as the largest contributor, the resistance of the current collectors is the most important one to reduce to lower the overall ESR. Improving the contact to the active material can yield up to a 1 Ω reduction in resistance. The distributed resistance, however, is not straightforward to reduce: it would be lowered by less porosity or a thinner layer of the active material, but the capacitance is then reduced as well. Optimizing the active layer thickness requires a compromise between the capacitance and ESR, and thus depends on the application usage of the supercapacitor.

The area-normalized ESR of the supercapacitors is on average 18 Ωcm^2, which is good compared to the previous reports summarized in Sec. 2.4. The devices reported by Keskinen et al. have much lower resistance, but utilize a metal current collector [13]. The very high resistance obtained with a metal current collector by Pettersson et al. is due to the low conductivity of the ionic liquid electrolytes [16]. Jost et al. did not use metal electrodes but were able to achieve a low ESR – similar to the results obtained here – with relatively thick carbon-fiber fabric [58]. However, the simplicity of printing the graphite current collector layer on a plastic substrate offers more versatility in terms of applications for the device.

4.1.2 Leakage and self-discharge

The leakage current of the screen-printed supercapacitors after a 1-hour hold at 0.9 V ranged from 2 to 4 µA and correlated well with the capacitance (Fig. 4.5). This is expected, as one major source of leakage is oxygen as an impurity, adsorbed on the surface of the carbon material [12, p. 561]: the more surface area there is, the more oxygen is introduced in the device. This is especially true for the supercapacitors prepared here, as all ink formulation, printing, drying and device assembly were done in ambient air. Other probable sources are residual metal contaminants in the carbon material and possibly reactive additives in the commercial graphite ink.

In our related work, Keskinen et al. [73] reported the self-discharge behaviour of supercapacitors similar to those presented here in detail. The conclusion was that the mechanism

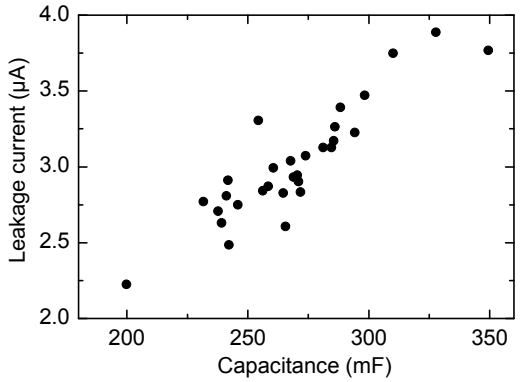

Figure 4.5: Leakage current of screen-printed supercapacitors plotted against device capacitance. Adapted from **IV**.

is a Faradaic reaction of impurities, as the open-circuit voltage decline was linear with respect to $\log(t)$. A barrier layer of aluminum was used outside these supercapacitors to prevent both water evaporation and oxygen permeation into the device. When devices were prepared without the barrier layer, the self-discharge was quicker than that of the devices with the barrier: the conclusion was that additional oxygen entering the device during the measurement period (one month) increases the rate of self-discharge further.

4.1.3 Complex capacitance

The complex capacitances of the screen-printed supercapacitors at each frequency were calculated from the impedance data through equations 2.4 given in Sec 2.3.2. Example plots for two samples are shown in Fig. 4.6a. It can be seen that the larger the real and complex parts of the capacitance are, the larger the device capacitance is; the value of C' at the lowest frequency corresponds well with the galvanostatically measured one.

The imaginary component, C'', describes losses occurring in the device; its maximum point reveals the characteristic time, τ_0, (reciprocal of the frequency), which is the time required to discharge the supercapacitor with 50% efficiency. Because the data points were sparse at the low-frequency end of the spectrum, a spline fit was made to the data to obtain a more accurate estimate of the maximum of C''. [**IV**]

The characteristic time results of the supercapacitors are presented in Fig. 4.6b. There is a clear dependence of τ_0 on capacitance, which is expected: a larger amount of charge stored takes a longer time to discharge, when the material is the same and only the layer thickness defines the capacitance. There is also a dependence on the ESR: the larger it is, the higher τ_0 is for a given capacitance value. The discharge times of the supercapacitors measured at 10 mA were a few seconds longer than the value of τ_0 for the corresponding sample. Thus, it can be concluded that the supercapacitors could be discharged with acceptable efficiency even at 10 mA. [**IV**]

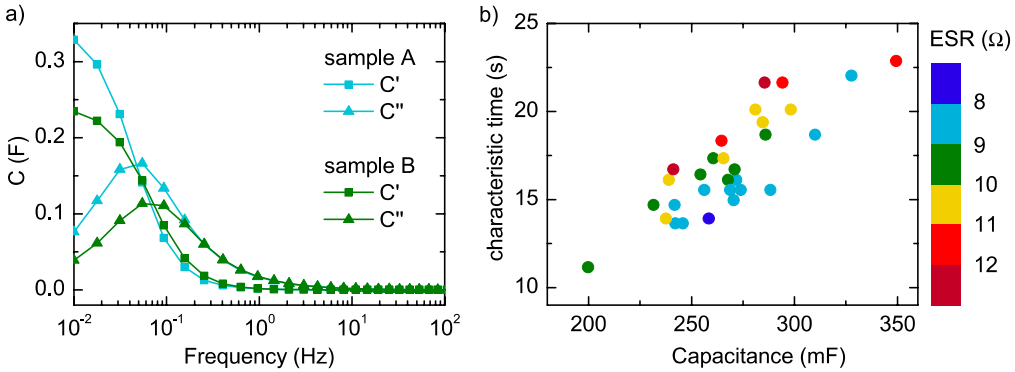

Figure 4.6: a) Complex capacitance of two screen-printed supercapacitor samples, A ($C = 328\,\mathrm{mF}$, $\mathrm{ESR} = 8.9\,\Omega$, $\tau_0 = 22\,\mathrm{s}$) and B ($C = 232\,\mathrm{mF}$, $\mathrm{ESR} = 9.0\,\Omega$, $\tau_0 = 15\,\mathrm{s}$). b) Characteristic time plotted against the capacitance with device ESR as the color scale. Adapted from **IV**.

4.2 Novel materials

4.2.1 Carbon nanotubes

The carbon nanotube ink was examined through scanning electron microscopy (SEM) and transmission electron microscopy (TEM) (Fig. 4.7a and b). The multi-walled nanotubes appear approximately 10 nm thick, as was specified by the supplier, and they are well-dispersed, forming a random network [**II**]. The structure of the assembled supercapacitor is shown in Fig. 4.7c; a 90° configuration was used, although there are no metallic current collectors.

Energy-dispersive X-ray spectroscopy (EDS) of the ink revealed the major impurities to be Na, Fe and Co, each of which was present at under 1 w-%. Na, possibly originating from the manufacture of the polymer dispersant, does not affect supercapacitor behaviour as it is also included in the electrolyte [**II**]. Fe and Co are most probably left in the CNT material during synthesis. They may cause leakage through electrochemical reactions, behaving as a "shuttle" between the positive and negative electrodes [12, p. 560].

The electrodes were approximately 13 – 16 µm thick but very uneven, with large open pores as well as denser areas. The sheet resistance was on average $15\,\Omega/\square$; at similar thickness, the graphite ink used as current collector in the AC supercapacitors would have sheet resistance of approximately $6\,\Omega/\square$. The porous and uneven structure of the CNT electrode may be one cause for the high resistance in addition to the insulating xylan dispersant; however, the porousness is needed when the same material doubles as the active layer.

The capacitance of the CNT supercapacitors was on average 12 mF, i.e., $6\,\mathrm{mF/cm^2}$. By comparison, Hu et al. reached $9.9\,\mathrm{mF/cm^2}$ with CNT ink printed on both sides of the separator [61]; however, they used single-walled carbon nanotubes, which are prohibitively expensive for use in real applications [28]. Multi-walled nanotubes, such as those used here, cost over \$50/kg [28]. This is still more expensive than activated carbon, but the price may decrease with the development of the production methods.

The ESR of the CNT supercapacitors was on average $80\,\Omega$, which is high especially compared to devices with metallic current collectors, but also to devices with only

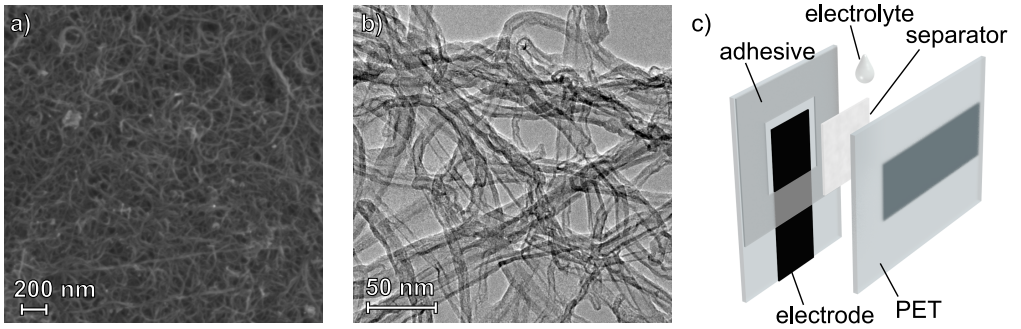

Figure 4.7: a) SEM and b) TEM images of the CNT ink. c) structure of the assembled supercapacitor. Adapted from **II**.

graphite ink as current collector. While the large sheet resistance of the CNT layers is one cause for the high ESR, another reason is the unoptimized geometry compared to the wide and short current collectors in the screen-printed AC supercapacitors. Thus, a simple configuration change could reduce the ESR to 30 – 40 Ω, based on the dependence in Fig. 4.2b.

The leakage current of the supercapacitors after a 30-minute voltage hold at 0.9 V was 7 µA. As the values for the screen-printed AC supercapacitors were reported from 1-hour voltage holds, the values are not comparable, because the leakage current falls during the measurement. Examining the current at 30 minutes into the first hold segment of the screen-printed supercapacitors, a value approximately double that of the CNT supercapacitors is found. However, the capacitance is in that case much larger (at least 20 times) – the leakage is then 10 times larger in the CNT supercapacitors in proportion to the capacitance of the device. One major reason is probably the presence of the Fe and Co impurities. More rigorous purification of the CNT material could thus decrease the leakage.

4.2.2 PEDOT-graphene composite

Poly(3,4-ethylenedioxythiophene) (PEDOT) composite materials were prepared on current collector electrodes with graphite ink on top of a metal layer. As a reference, only PEDOT was electropolymerized on the current collector; a composite of PEDOT and graphene oxide (GO) was deposited similarly, with the negatively charged GO sheets acting as counterions in the electropolymerization. A composite of PEDOT and reduced graphene oxide (rGO) was formed through electrochemical reduction of PEDOT/GO. Details of the film characterization in a 3-electrode setup, as well as SEM images of the films, are in **III**.

Symmetric supercapacitors were prepared from the material, as PEDOT can function as both the negative and positive electrode [74]. The results obtained for these supercapacitors are shown in Table 4.2. The single-electrode values should be approximately double that of the device values, when reporting capacitance instead of specific capacitance, but that is not the case here, probably due to the different electrolyte and voltage ranges used. The capacitance of the PEDOT devices is similar to that obtained by Österholm et al. [74] with similar electropolymerized PEDOT layers, assembled into symmetric supercapacitors.

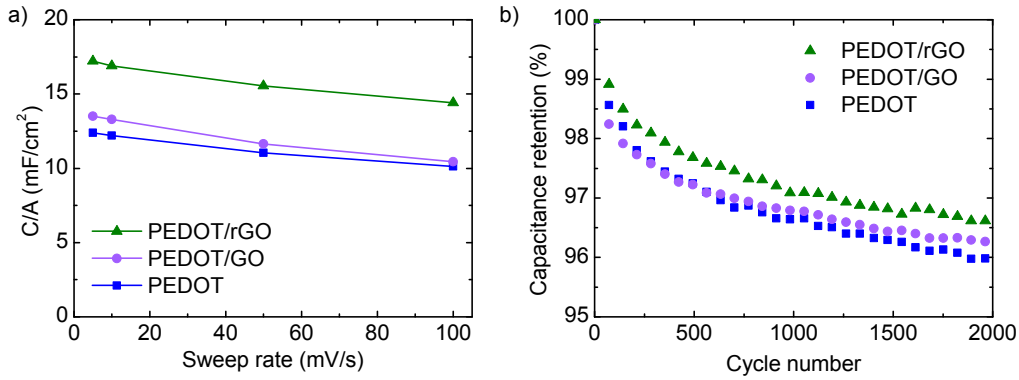

Figure 4.8: a) Capacitances of the PEDOT and composite supercapacitors, calculated from CV curves. b) Capacitance retention during cycling at 50 mV/s. Adapted from **III**.

Table 4.2: Results of the PEDOT composite electrodes and supercapacitors. C_{se} denotes single-electrode capacitance, measured in IL against Ag/AgCl from −0.4 V to +0.8 V. Other values are from symmetric devices with NaCl (aq) electrolyte. CV capacitances are calculated from the charging phase of the 100 mV/s sweep. Adapted from **III**.

	PEDOT	PEDOT/GO	PEDOT/rGO
C_{se} in IL (mF/cm^2)	11	16	25
C (mF/cm^2) from CV	10	10	14
C (mF/cm^2) from GCD	14	14	18
ESR (Ω)	26	43	25

In the single-electrode values, the capacitance increases with the incorporation of GO to the PEDOT material, which is not observed in the device results. As GO is not an electrical conductor, it is not likely that it is taking part in double-layer formation. Instead, it may be that GO changes the morphology of the PEDOT film to a more porous one, such that the large ions of the ionic liquid are better able to access the material. On the other hand, the smaller, more mobile Na^+ and Cl^- ions in the aqueous electrolyte may be able to move in the PEDOT layer better even without the GO. [**III**]

The reduction of GO to rGO improves the capacitance because the partially restored conductivity of the graphene layers allows them to participate in double-layer formation. The CV measurement yields a somewhat lower value compared to the GCD measurement, which can, at least partly, be explained through the slower discharge used in the GCD measurement. The discharge rate was approximately 3.5 mV/s in GCD. The capacitance obtained from the CV measurements at different voltage sweep rates are shown in Fig. 4.8a; the values increase with decreasing sweep rate.

The ESR of the PEDOT devices was on average 26 Ω. Addition of the non-conductive GO nearly doubles the ESR, while the reduction to rGO returns the resistance to that of the bare PEDOT devices. The incorporation of rGO into the film does not reduce the ESR further, which could indicate that most of the ESR originates from parts of the device other than the active material, even with metallic current collectors. The main

benefit of rGO is then the approximately 30% increase in capacitance compared to bare PEDOT, due to the added surface area capable of double-layer formation. [**III**]

The cycling stability of the devices is fairly good with 5 – 7% drop in capacitance after 2000 cycles at 50 mV/s, calculated from GCD before and after the cycling. The evolution of the capacitance during cycling, calculated from the CV curves, is shown in Fig. 4.8b. There are no significant differences between the sample types; PEDOT/GO yields the lowest capacitance drop after the cycling. It is possible that some electrochemical reduction of the GO to rGO takes place during the cycling as well as during the 30-minute voltage hold prior to the galvanostatic discharge. The difference is, however, too small to make a definitive conclusion. In general, the cycling stability of conducting polymers is lower in aqueous electrolytes than in ionic liquids [35], which explains the better stability of similar devices with ionic liquid electrolyte [74]. However, using aqueous electrolytes brings the advantages of facile processing and use of the devices.

4.3 Measurement parameter effects

4.3.1 Rate dependence

Many factors can influence the results of supercapacitor measurements; one such effect is seen in Fig. 4.8a, where a slower CV sweep rate produces a higher capacitance. One cause for this is the different migration time of the electrolyte ions in the pores of the electrode – with a slower rate, the full surface area of the active material is in use. With pseudocapacitive materials, the reaction time scale may also cause some delay in the response of the device. Similarly to CV, a lower measurement current in GCD should also yield a higher capacitance, and this is frequently observed [75].

In **II**, lower measurement current did not yield a higher capacitance, but in fact a lower one. The effect was studied with a simple circuit model, where the supercapacitor was represented by a capacitor, a series resistor and a parallel leakage resistance of 130 kΩ (Fig. 4.9a). The leakage resistance was determined from the value of the measured leakage current at 0.9 V. A simulation with a 30-minute voltage hold and a discharge at constant current was run, and the resulting discharge curve used for capacitance calculation similarly to measured results. The capacitances at different currents, both measured and simulated, are shown in Fig. 4.9b.

Stoller and Ruoff [48] note that when the measurement current is on the order of the leakage current, the latter may interfere with the results. This is indeed observed here, as the apparent capacitance begins to fall when the measurement current is approximately three times the leakage current (7 µA) at 0.9 V. In reality, the leakage "resistance" is voltage-dependent, with a higher resistance at lower voltages due to the likely Faradaic origin of the leakage. Yet, even a very simple model such as the one used here yields results close to the measured data.

4.3.2 Maximum voltage

The operating voltage of a supercapacitor is a very important parameter which affects the performance of the device. Screen-printed AC supercapacitors were used in testing the effect of the voltage on the capacitance and the leakage current [**IV**]. In an initial test, the same device was charged to different maximum voltages from 0.8 V to 1.2 V and the capacitance calculated from GCD after a 30-minute hold at the respective voltages.

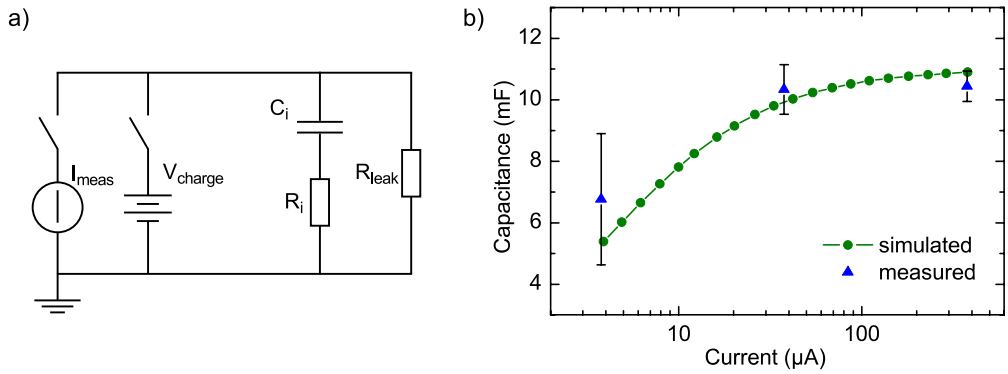

Figure 4.9: a) The circuit used in simulating the effect of discharge current on capacitance; $C_i = 11\,\mathrm{mF}$, $R_i = 100\,\Omega$, and $R_L = 130\,\mathrm{k}\Omega$. b) Simulated and measured capacitance results calculated from galvanostatic discharge at different currents. Adapted from **II**.

Because the measurement affects the device, the voltage cycle was repeated eight times, resulting in 40 cycles in total. The results are shown in Fig. 4.10a.

The difference in the initial capacitance values is large: the capacitance rises 10% from the initial 0.8 V value to the 1.2 V one. However, the most interesting observation is that the capacitances measured at different voltages seem to converge: the low-V ones increase with cycling and the high-V ones decrease. At higher voltages, a significant part of the capacitance probably originates from pseudocapacitance of, e.g., oxygen and oxygen-containing fuctional groups. With cycling – each cycle includes a 30-minute hold segment – the impurities may become depleted, resulting in a fall in capacitance. The rise in capacitance at the lower voltages, at the same time as the capacitance at higher voltages is decreasing, may be related to initial conditioning of the supercapacitor, e.g., through changes in surface chemistry. Slight initial increase in the capacitance during cycling has been observed also in our related publication by Keskinen et al. [73]. Ruiz et al. have previously reported the increase of capacitance with operating voltage, but do not mention if cycling the same device at different voltages affects the results [75].

To discern the effects of changing the voltage from the effects of cycling, separate batches of samples were measured at voltages 0.8 V, 1.0 V and 1.2 V. The resulting capacitances, plotted against the AC mass in the device, are shown in Fig. 4.10b. While there is no significant difference between the capacitances measured at 0.8 V and 1.0 V, the values of the 1.2 V measurement are approximately 10% higher for a given AC mass. Clearly, there is a pseudocapacitive component which becomes active at voltages between 1.0 V and 1.2 V.

The effect of the maximum voltage on supercapacitor aging was also examined; half of the samples were cycled 100 times and the other half held at the maximum voltage for 24 h. The capacitances were measured again after this and the relative changes are presented in Table 4.3. Consistent with the results reported by Weingarth et al. [53], the voltage hold test results in a quicker aging. The effect is most clearly visible for the samples measured at 1.2 V.

At 1.0 V, there is a slight increase in the capacitance after the cycling; it is possible that the initial conditioning processes increasing the capacitance, observed in the voltage-cycling test of Fig. 4.10a, are visible here as well. As the effect is not seen in the 0.8 V results,

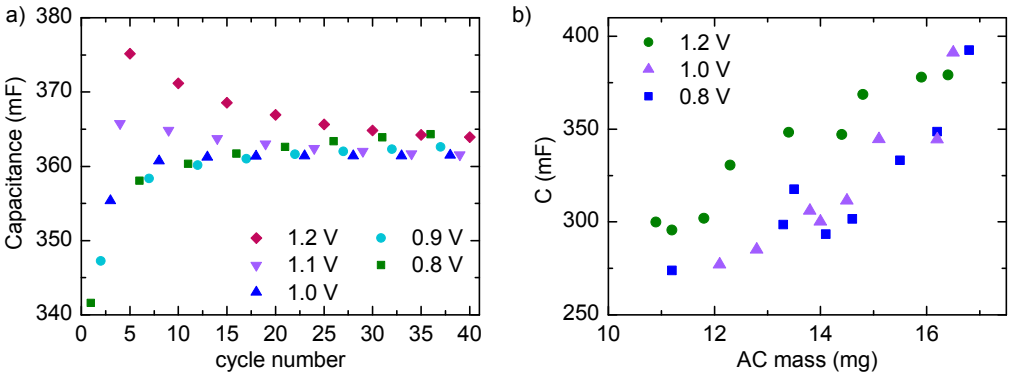

Figure 4.10: a) Capacitances calculated from GCD after voltage hold at different voltages; a single sample was consecutively cycled from 0.8 V to 1.2 V at 0.1 V intervals and held at the maximum voltage for 30 minutes before discharge. b) Capacitance versus AC mass for samples measured with GCD at different voltages. Each data point is a separate sample. Adapted from **IV**.

Table 4.3: Average change in capacitance in sample sets measured at different voltages before and after cycling or voltage hold.

	0.8 V	1.0 V	1.2 V
cycling	−0.4%	+0.2%	−1.5 %
hold	−0.5%	−1.4%	−4.6%

it can be concluded that the processes may require a voltage higher than 0.8 V, or a longer cycling when the lower voltage is used. At 1.2 V, the degradation is too quick for observing this slight initial improvement.

The leakage current was again found to increase with increasing capacitance for a given measurement voltage, but the difference between voltages was greater than that between samples of different AC masses. The leakage current is approximately three times higher for the samples measured at 1.2 V (9–12 µA) than for samples measured at 0.8 V (2–4 µA). After cycling, the leakage current is reduced by approximately 30% with all the voltages, and after the voltage hold test – with different samples – by 60%. [**IV**]

Based on the aging behaviour and leakage properties of the screen-printed aqueous supercapacitors, it can be concluded that a maximum voltage of 1.0 V would be suitable for final applications. While 1.2 V does produce a higher capacitance initially, the degradation is so much quicker that for reliable and repeatable capacitor behaviour a lower voltage is preferable.

4.4 Energy harvesting

Energy harvesting was demonstrated in **I** and **III** with simple demonstrations which show the feasibility of using the supercapacitors in an energy harvester application. Further examples with similar supercapacitors are reported in our related publications by Tuukkanen et al. [76] and Pörhönen et al. [77].

4.4.1 RF harvester with ASIC voltage regulation

Two AC supercapacitors with metal/graphite current collectors were connected in series and charged with a printed RF harvester consisting of a printed antenna, a printed organic diode and a printed capacitor. The supercapacitor sizes were 4 cm^2 and 2 cm^2, with capacitances 450 mF and 210 mF, respectively. The input transmitter for the harvester antenna was adjusted between two distances from the RF source, one yielding a higher input and another a lower one.

The supercapacitors were charged to 1.8 V (2 × 0.9 V) and disconnected from the harvester. The charging curves are shown in Fig. 4.11a. While the capacitor size obviously affected the charging rate, the input magnitude was also important: the charging time was 22 min at high input and 2.3 h at low input for the 4 cm^2 devices. The charging was faster in the beginning than close to the maximum voltage. One reason may be leakage current of the supercapacitors, but another is the voltage over the diode: when the charging is begun, the supercapacitor initially appears as a short circuit. When the supercapacitor voltage rises, the voltage over the diode is reduced, reducing the output current and thus the supercapacitor charging rate.

The charged supercapacitors were connected to the ASIC input and the voltage monitored (Fig. 4.11b). The ASIC gave a steady output of 1.2 V for input voltages down to 0.78 V. A significant difference can be seen between the different charging rate cases; the 4 cm^2 devices yield a nearly 8-hour operation time when charged quickly, but well over 10 hours when charged with a low rate. This is due to the charge redistribution effect: with a quick charge, the AC surface is not evenly covered with ions. After the quick charging is terminated, ions continue to migrate further down the pores, decreasing the observed voltage over the devices. The observed operation time of the supercapacitors and ASIC would already be nearly enough to power a small sensor overnight.

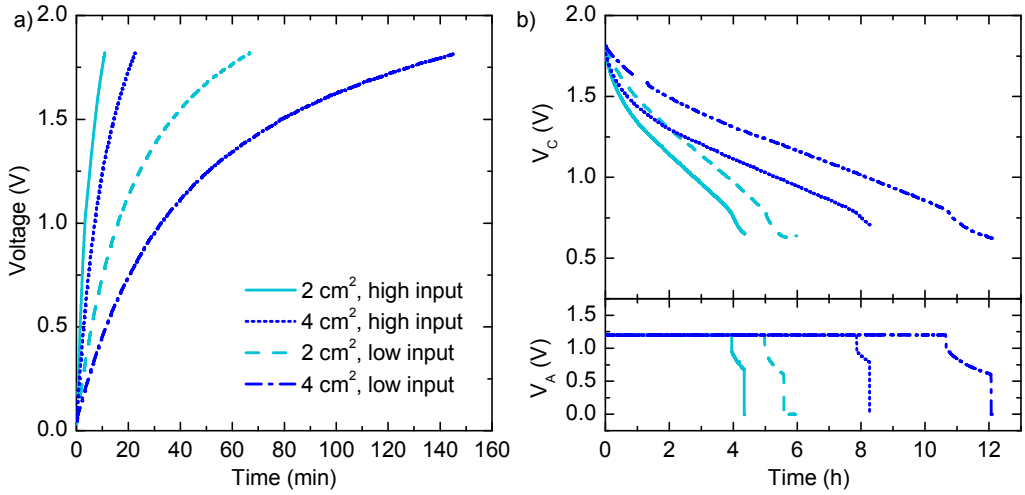

Figure 4.11: a) Charging curves of the two series-connected supercapacitors, with two device sizes at high and low input fields. b) Operation of the ASIC with 1 MΩ load by the charged supercapacitors. The supercapacitor voltage is denoted V_C and the ASIC output voltage V_A. Adapted from **I**.

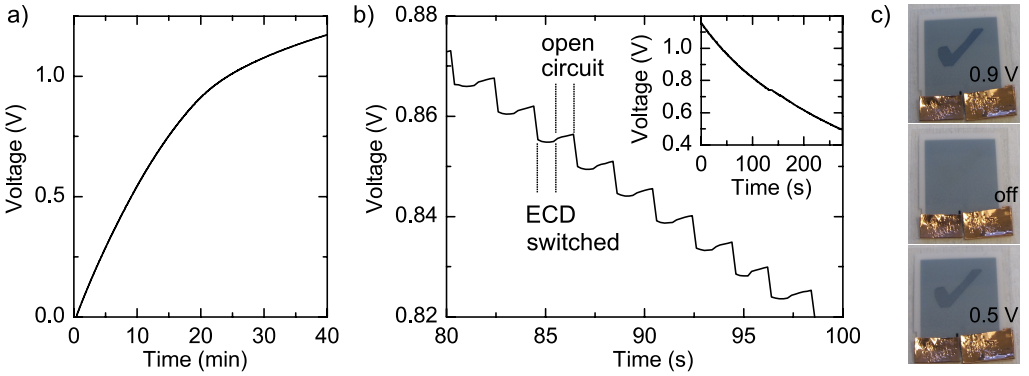

Figure 4.12: a) Charging curve of the supercapacitor when charged with the OPV module. b) Voltage over the supercapacitor during the ECD switching. c) The ECD in the on and off states, and the limit of clear image at 0.5 V. Adapted from **III**.

4.4.2 OPV harvester and ECD demonstration

A PEDOT/rGO supercapacitor was used in a harvester with a printed organic photovoltaic (OPV) module and a printed electrochromic display (ECD). The supercapacitor was charged with the OPV indoors with ambient workspace lighting. As was observed with the RF harvester, the charging was quicker in the beginning compared to the end of charging (Fig. 4.12a). However, as the IV curve of the OPV module [72] indicates, the current should not decrease considerably in the voltage interval used here; rather, it is probable that device leakage is the main cause for the decreasing charging rate. A maximum voltage of nearly 1.2 V was used to ensure the device was completely charged.

Once charged, the supercapacitor was disconnected from the OPV module and connected to the ECD. The device was switched on and off every two seconds by reversing the connection; the leads were kept connected for one second, and the display on open circuit for another second. A segment of the discharge curve is shown in Fig. 4.12b. It can be seen that the voltage falls approximately 6 mV on each switch, on both switching directions. During the one-second open circuit, the voltage rises slightly. This may be related to charge reorganization; the slower parts of the supercapacitor electrodes compensate charge drawn quickly from the most accessible parts, resulting in an overall increase in observed voltage. The display switching was rapid, with no delay apparent to the naked eye.

In total, 65 on-and-off cycles were achieved before the display image was no longer clear at around 0.5 V (Fig. 4.12c). In fact, switching off the ECD would not require a negative potential – a short circuit would suffice – so the number of cycles could be doubled. As the capacitor used here had a capacitance of only 36 mF, a longer operation time could also be achieved with the AC supercapacitors reported in the previous sections.

5 Summary and outlook

The need for printable, low-cost energy storage solutions is growing due to the increase in distributed and ubiquitous electronics. Placing billions of sensors and other electronic devices everywhere in our surroundings calls for an autonomous energy source, i.e., harvesting the energy from the ambient environment. The supercapacitors presented in this thesis offer an excellent option for the interim storage of the harvested energy: they are cheap, printable, potentially flexible, and have a good cycling stability. The devices can be safely placed in any environment as they have no toxic components, and they can be disposed of, e.g., through incineration.

The thesis studied different types of printed and coated supercapacitors. Currently, the conventional activated carbon material yields the best results due to its highest performance as well as low cost. However, there are intensive efforts to develop nanostructured materials which could surpass the performance of activated carbon. One such material is carbon nanotubes, which not only have a high surface area, but also good conductivity. It was shown in this thesis that an ink formulated from CNTs can be used in supercapacitor electrodes in such a way that it is the only electrode layer, doubling as both the current collector and the active material, which simplifies the fabrication process. The capacitance reached with the CNT supercapacitors was $6\,\mathrm{mF/cm^2}$ and the ESR $80\,\Omega$. While not yet competetive with activated carbon, further developments in the synthesis, purification and dispersion methods could produce better devices.

Another interesting direction of supercapacitor material development are composites of conductive polymers, i.e., pseudocapacitive materials, and carbon nanomaterials. An electropolymerized composite, PEDOT and reduced graphene oxide, was studied in this thesis. It was fabricated directly on the blade-coated current collector electrodes and used in a symmetric supercapacitor; the succesful scale-up of the electropolymerization from the conventional millimetre-sized electrodes used in electropolymerization on printable electrodes shows the potential of the method in larger-scale manufacturing. The capacitance was $18\,\mathrm{mF/cm^2}$ and ESR $25\,\Omega$. The addition of the reduced graphene oxide improved the capacitance 30% compared to that of devices prepared with only PEDOT layers.

Screen-printed activated carbon based supercapacitors reached on average a capacitance of $150\,\mathrm{mF/cm^2}$ and ESR of $10\,\Omega$. In the short term, this material is the most interesting direction for the development of printable supercapacitors. The properties were studied in more detail over a large sample set with different layer thicknesses: it was found that the specific capacitance decreases somewhat with the activated carbon mass and that the magnitude of the leakage current is directly related to the capacitance. Current collectors consisting only of graphite ink were found to be the main source of the device ESR. More detailed analysis of the device resistances though impedance spectroscopy revealed the

sources to be:

- resistance of the current collectors and bulk electrolyte: 6 – 9 Ω,
- contact resistance between the active material and the current collector: 0.5 – 1.1 Ω and
- distributed resistance of the electrolyte and the active material in the porous electrode: 0.8 – 1.5 Ω.

The maximum voltage was found to have a great effect on the capacitance, leakage and the device stability, with higher voltage yielding higher capacitance but also larger leakage and quicker device degradation. Based on the results, a suitable compromise for the maximum voltage is 1.0 V.

Demonstrations of the supercapacitors in energy harvesting were carried out with both RF and light harvesting, and the performance of the supercapacitors was found suitable for powering a small electronic device such as an electrochromic display. An essential part of any harvester containing a supercapacitor is a voltage control circuit, which can produce a steady output from a supercapacitor where the voltage declines linearly on discharge. Over 10 hours of operation was demonstrated with an application-specific integrated circuit.

Important issues which need to be addressed in the future are the flexibility and shelf-life of the printed supercapacitors. Packaging and sealing the supercapacitors with aqueous electrolyte in such a way that the device does not dry out is crucial for long-term operation. The flexibility of the devices presents even more requirements for durable packaging. Another future challenge is decreasing the ESR of the devices; as was found in this thesis, this practically means improving the conductivity of the current collectors. A metal layer is problematic not only due to issues with disposability, but also due to the corrosion in the case of defects in the graphite layer. Using only graphite yields approximately 10 Ω device resistances, which may still be too high in applications with high peak power demand. Better inks could be found from commercial sources or fabricated in-house; for example, carbon nanotubes as ink additives could provide the needed increase in conductivity. Overall, while the basic structure of the supercapacitors has here been demonstrated to work well, future development of the materials and packaging should improve the usability in applications further.

Bibliography

[1] R. Vullers, R. van Schaijk, I. Doms, C. Van Hoof, and R. Mertens, "Micropower energy harvesting," *Solid-State Electron.*, vol. 53, no. 7, pp. 684–693, 2009.

[2] C. O. Mathuna, T. O'Donnell, R. V. Martinez-Catala, J. Rohan, and B. O'Flynn, "Energy scavenging for long-term deployable wireless sensor networks," *Talanta*, vol. 75, no. 3, pp. 613–623, 2008.

[3] J. A. Stankovic, "Research directions for the Internet of Things," *IEEE Internet Things J.*, vol. 1, no. 1, pp. 3–9, 2014.

[4] H. Jayakumar, K. Lee, W. S. Lee, A. Raha, Y. Kim, and V. Raghunathan, "Powering the Internet of Things," in *Proc. 2014 International Symposium on Low Power Electronics and Design*. ACM, 2014, pp. 375–380.

[5] P. Kamalinejad, C. Mahapatra, Z. Sheng, S. Mirabbasi, V. C. Leung, and Y. L. Guan, "Wireless energy harvesting for the internet of things," *IEEE Commun. Mag.*, vol. 53, no. 6, pp. 102–108, 2015.

[6] R. Want, K. I. Farkas, and C. Narayanaswami, "Guest editors' introduction: Energy harvesting and conservation," *IEEE Pervasive Comput.*, vol. 4, no. 1, pp. 14–17, 2005.

[7] J. A. Paradiso and T. Starner, "Energy scavenging for mobile and wireless electronics," *IEEE Pervasive Comput.*, vol. 4, no. 1, pp. 18–27, 2005.

[8] J. Gubbi, R. Buyya, S. Marusic, and M. Palaniswami, "Internet of Things (IoT): A vision, architectural elements, and future directions," *Future Gener. Comp. Sy.*, vol. 29, no. 7, pp. 1645–1660, 2013.

[9] D. Miorandi, S. Sicari, F. De Pellegrini, and I. Chlamtac, "Internet of things: Vision, applications and research challenges," *Ad Hoc Networks*, vol. 10, no. 7, pp. 1497–1516, 2012.

[10] V. Raghunathan, S. Ganeriwal, and M. Srivastava, "Emerging techniques for long lived wireless sensor networks," *IEEE Commun. Mag.*, vol. 44, no. 4, pp. 108–114, 2006.

[11] J. Wen, Y. Yu, and C. Chen, "A review on lithium-ion batteries safety issues: existing problems and possible solutions," *Mater. Express*, vol. 2, no. 3, pp. 197–212, 2012.

[12] B. E. Conway, *Electrochemical Supercapacitors: Scientific Fundamentals and Technological Applications*. New York: Kluwer Academic / Plenum Publishers, 1999.

[13] J. Keskinen, E. Sivonen, S. Jussila, M. Bergelin, M. Johansson, A. Vaari, and M. Smolander, "Printed supercapacitors on paperboard substrate," *Electrochim. Acta*, vol. 85, pp. 302 – 306, 2012.

[14] F. Gonzales, "Supercapacitor Technologies and Markets 2016-2026," IDTechEx, Tech. Rep., 2016.

[15] M. Kaempgen, C. K. Chan, J. Ma, Y. Cui, and G. Gruner, "Printable thin film supercapacitors using single-walled carbon nanotubes," *Nano Lett.*, vol. 9, no. 5, pp. 1872 – 1876, 2009.

[16] F. Pettersson, J. Keskinen, T. Remonen, L. Von Hertzen, E. Jansson, K. Tappura, Y. Zhang, C.-E. Wilén, and R. Österbacka, "Printed environmentally friendly supercapacitors with ionic liquid electrolytes on paper," *J. Power Sources*, vol. 271, pp. 298 – 304, 2014.

[17] V. L. Pushparaj, M. M. Shaijumon, A. Kumar, S. Murugesan, L. Ci, R. Vajtai, R. J. Linhardt, O. Nalamasu, and P. M. Ajayan, "Flexible energy storage devices based on nanocomposite paper," *P. Natl. Acad. Sci.*, vol. 104, no. 34, pp. 13 574 – 13 577, 2007.

[18] J. S. Sagu, N. York, D. Southee, and K. Wijayantha, "Printed electrodes for flexible, light-weight solid-state supercapacitors – a feasibility study," *Circuit World*, vol. 41, no. 2, pp. 80 – 86, 2015.

[19] J. R. Miller, "Market and Applications of Electrochemical Capacitors," in *Supercapacitors: Materials, Systems and Applications*, F. Beguin, E. Frackowiak, and M. Lu, Eds. John Wiley & Sons, 2013.

[20] R. Kötz and M. Carlen, "Principles and applications of electrochemical capacitors," *Electrochim. Acta*, vol. 45, no. 15-16, pp. 2483 – 2498, 2000.

[21] S. W. Donne, "General Principles of Electrochemistry," in *Supercapacitors: Materials, Systems and Applications*, F. Beguin, E. Frackowiak, and M. Lu, Eds. John Wiley & Sons, 2013.

[22] W. G. Pell and B. E. Conway, "Peculiarities and requirements of asymmetric capacitor devices based on combination of capacitor and battery-type electrodes," *J. Power Sources*, vol. 136, no. 2, pp. 334 – 345, 2004.

[23] H. A. Andreas, "Self-discharge in electrochemical capacitors: A perspective article," *J. Electrochem. Soc.*, vol. 162, no. 5, pp. A5047 – A5053, 2015.

[24] R. De Levie, "On porous electrodes in electrolyte solutions: I. capacitance effects," *Electrochim. Acta*, vol. 8, no. 10, pp. 751 – 780, 1963.

[25] J. Chmiola, G. Yushin, Y. Gogotsi, C. Portet, P. Simon, and P.-L. Taberna, "Anomalous increase in carbon capacitance at pore sizes less than 1 nanometer," *Science*, vol. 313, no. 5794, pp. 1760 – 1763, 2006.

[26] G. V. Merrett and A. S. Weddell, "Supercapacitor leakage in energy-harvesting sensor nodes: Fact or fiction?" in *Ninth International Conference on Networked Sensing Systems (INSS)*. IEEE, 2012, pp. 1 – 5.

[27] P. J. Hall, M. Mirzaeian, S. I. Fletcher, F. B. Sillars, A. J. Rennie, G. O. Shitta-Bey, G. Wilson, A. Cruden, and R. Carter, "Energy storage in electrochemical capacitors: designing functional materials to improve performance," *Energy Environ. Sci.*, vol. 3, no. 9, pp. 1238 – 1251, 2010.

[28] L. Weinstein and R. Dash, "Supercapacitor carbons – have exotic carbons failed?" *Mater. Today*, vol. 16, no. 10, pp. 356 – 357, 2013.

[29] A. G. Pandolfo and A. F. Hollenkamp, "Carbon properties and their role in supercapacitors," *J. Power Sources*, vol. 157, no. 1, pp. 11 – 27, 2006.

[30] P. Simon and Y. Gogotsi, "Materials for electrochemical capacitors," *Nat. Mater.*, vol. 7, no. 11, pp. 845 – 854, 2008.

[31] X. Du, P. Guo, H. Song, and X. Chen, "Graphene nanosheets as electrode material for electric double-layer capacitors," *Electrochim. Acta*, vol. 55, no. 16, pp. 4812 – 4819, 2010.

[32] D. R. Dreyer, S. Park, C. W. Bielawski, and R. S. Ruoff, "The chemistry of graphene oxide," *Chem. Soc. Rev.*, vol. 39, no. 1, pp. 228 – 240, 2010.

[33] R. Raccichini, A. Varzi, S. Passerini, and B. Scrosati, "The role of graphene for electrochemical energy storage," *Nat. Mater.*, vol. 14, no. 3, pp. 271 – 279, 2015.

[34] B. Conway, "Impedance Behaviour of Electrochemical Supercapacitors and Porous Electrodes," in *Impedance Spectroscopy: Theory, Experiment, and Applications*, E. Barsoukov and J. R. Macdonald, Eds. John Wiley & Sons, 2005.

[35] G. A. Snook, P. Kao, and A. S. Best, "Conducting-polymer-based supercapacitor devices and electrodes," *J. Power Sources*, vol. 196, no. 1, pp. 1 – 12, 2011.

[36] T. Pandolfo, V. Ruiz, S. Sivakkumar, and J. Nerkar, "General Properties of Electrochemical Capacitors," in *Supercapacitors: Materials, Systems and Applications*, F. Beguin, E. Frackowiak, and M. Lu, Eds. John Wiley & Sons, 2013.

[37] P. Azaïs, "Manufacturing of Industrial Supercapacitors," in *Supercapacitors: Materials, Systems and Applications*, F. Beguin, E. Frackowiak, and M. Lu, Eds. John Wiley & Sons, 2013.

[38] L. Demarconnay, E. Raymundo-Pinero, and F. Béguin, "A symmetric carbon/carbon supercapacitor operating at 1.6 V by using a neutral aqueous solution," *Electrochem. Commun.*, vol. 12, no. 10, pp. 1275 – 1278, 2010.

[39] T. Brousse, D. Belanger, and D. Guay, "Asymmetric and Hybrid Devices in Aqueous Electrolytes," in *Supercapacitors: Materials, Systems and Applications*, F. Beguin, E. Frackowiak, and M. Lu, Eds. John Wiley & Sons, 2013.

[40] Q. Gao, L. Demarconnay, E. Raymundo-Piñero, and F. Béguin, "Exploring the large voltage range of carbon/carbon supercapacitors in aqueous lithium sulfate electrolyte," *Energy Environ. Sci.*, vol. 5, no. 11, pp. 9611 – 9617, 2012.

[41] I. Krossing, J. Slattery, C. Daguenet, P. Dyson, A. Oleinikova, and H. Weingärtner, "Why are ionic liquids liquid? a simple explanation based on lattice and solvation energies," *J. Am. Chem. Soc.*, vol. 128, no. 41, pp. 13 427 – 13 434, 2006.

[42] M. Earle and K. Seddon, "Ionic liquids. green solvents for the future," *Pure Appl. Chem.*, vol. 72, no. 7, pp. 1391 – 1398, 2000.

[43] C.-C. Yang, S.-T. Hsu, and W.-C. Chien, "All solid-state electric double-layer capacitors based on alkaline polyvinyl alcohol polymer electrolytes," *J. Power Sources*, vol. 152, pp. 303 – 310, 2005.

[44] C. Meng, C. Liu, L. Chen, C. Hu, and S. Fan, "Highly flexible and all-solid-state paperlike polymer supercapacitors," *Nano Lett.*, vol. 10, no. 10, pp. 4025 – 4031, 2010.

[45] S. Zhang and N. Pan, "Supercapacitors performance evaluation," *Adv. Energy Mater.*, vol. 5, no. 6, p. 1401401, 2015, 1401401.

[46] International Electrotechnical Comission, "International standard: Fixed electric double layer capacitors for use in electronic equipment, IEC 62391-1," 2006.

[47] A. Burke, "Testing of Electrochemical Capacitors," in *Supercapacitors: Materials, Systems and Applications*, F. Beguin, E. Frackowiak, and M. Lu, Eds. John Wiley & Sons, 2013.

[48] M. D. Stoller and R. S. Ruoff, "Best practice methods for determining an electrode material's performance for ultracapacitors," *Energy Environ. Sci.*, vol. 3, no. 9, pp. 1294 – 1301, 2010.

[49] J. R. Macdonald and W. B. Johnson, "Fundamentals of Impedance Spectroscopy," in *Impedance Spectroscopy: Theory, Experiment, and Applications*, E. Barsoukov and J. R. Macdonald, Eds. John Wiley & Sons, 2005.

[50] P. Taberna, P. Simon, and J.-F. Fauvarque, "Electrochemical characteristics and impedance spectroscopy studies of carbon-carbon supercapacitors," *J. Electrochem. Soc.*, vol. 150, no. 3, pp. A292 – A300, 2003.

[51] C. Portet, P. Taberna, P. Simon, and C. Laberty-Robert, "Modification of Al current collector surface by sol – gel deposit for carbon – carbon supercapacitor applications," *Electrochim. Acta*, vol. 49, no. 6, pp. 905 – 912, 2004.

[52] J. R. Miller, "Reliability of Electrochemical Capacitors," in *Supercapacitors: Materials, Systems and Applications*, F. Beguin, E. Frackowiak, and M. Lu, Eds. John Wiley & Sons, 2013.

[53] D. Weingarth, A. Foelske-Schmitz, and R. Kötz, "Cycle versus voltage hold – which is the better stability test for electrochemical double layer capacitors?" *J. Power Sources*, vol. 225, pp. 84 – 88, 2013.

[54] H. Gualous and R. Gallay, "Supercapacitor Module Sizing and Heat Management under Electric. Thermal and Aging Constraints," in *Supercapacitors: Materials, Systems and Applications*, F. Beguin, E. Frackowiak, and M. Lu, Eds. John Wiley & Sons, 2013.

[55] C. M. Lungoci and I. D. Oltean, "Comparative analysis for the supercapacitors packaging characteristics," in *Design and Technology in Electronic Packaging (SIITME), 2010 IEEE 16th International Symposium for*. IEEE, 2010, pp. 93 – 98.

[56] Y. Zhan, Y. Mei, and L. Zheng, "Materials capability and device performance in flexible electronics for the Internet of Things," *J. Mater. Chem. C*, vol. 2, no. 7, pp. 1220 – 1232, 2014.

[57] A. B. Dighe, D. P. Dubal, and R. Holze, "Screen printed asymmetric supercapacitors based on $LiCoO_2$ and graphene oxide," *Z. Anorg. Allg. Chem.*, vol. 640, no. 14, pp. 2852 – 2857, 2014.

[58] K. Jost, D. Stenger, C. R. Perez, J. K. McDonough, K. Lian, Y. Gogotsi, and G. Dion, "Knitted and screen printed carbon-fiber supercapacitors for applications in wearable electronics," *Energy Environ. Sci.*, vol. 6, no. 9, pp. 2698 – 2705, 2013.

[59] C. C. Ho, D. Steingart, J. Evans, and P. Wright, "Tailoring electrochemical capacitor energy storage using direct write dispenser printing," *ECS Trans.*, vol. 16, no. 1, pp. 35 – 47, 2008.

[60] A. Somov, C. C. Ho, R. Passerone, J. W. Evans, and P. K. Wright, "Towards extending sensor node lifetime with printed supercapacitors," in *Wireless Sensor Networks, Proc. 9th European Conference, EWSN 2012, Trento, Italy, February 15-17, 2012*, G. P. Picco and W. Heinzelman, Eds. Springer, 2012, pp. 212 – 227.

[61] L. Hu, H. Wu, and Y. Cui, "Printed energy storage devices by integration of electrodes and separators into single sheets of paper," *Appl. Phys. Lett.*, vol. 96, no. 18, pp. 183 502 – 183 502, 2010.

[62] S. Cho, M. Kim, and J. Jang, "Screen-printable and flexible RuO_2 nanoparticle-decorated PEDOT:PSS/graphene nanocomposite with enhanced electrical and electrochemical performances for high-capacity supercapacitor," *ACS Appl. Mater. Interfaces*, vol. 7, no. 19, pp. 10 213 – 10 227, 2015.

[63] D. Qi, Y. Liu, Z. Liu, L. Zhang, and X. Chen, "Design of architectures and materials in in-plane micro-supercapacitors: Current status and future challenges," *Advanced Materials*, 2016.

[64] J. Li, V. Mishukova, and M. Östling, "All-solid-state micro-supercapacitors based on inkjet printed graphene electrodes," *Appl. Phys. Lett.*, vol. 109, no. 12, p. 123901, 2016.

[65] L. Nyholm, G. Nyström, A. Mihranyan, and M. Strømme, "Toward flexible polymer and paper-based energy storage devices," *Adv. Mater.*, vol. 23, no. 33, pp. 3751 – 3769, 2011.

[66] H. Zhang, Y. Qiao, and Z. Lu, "Fully printed ultraflexible supercapacitor supported by a single-textile substrate," *ACS Appl. Mater. Interfaces*, vol. 8, no. 47, pp. 32 317 – 32 323, 2016.

[67] S. K. Ujjain, P. Ahuja, R. Bhatia, and P. Attri, "Printable multi-walled carbon nanotubes thin film for high performance all solid state flexible supercapacitors," *Mater. Res. Bull.*, vol. 83, pp. 167 – 171, 2016.

[68] M. H. Ervin, L. T. Le, and W. Y. Lee, "Inkjet-printed flexible graphene-based supercapacitor," *Electrochim. Acta*, vol. 147, pp. 610 – 616, 2014.

[69] C. Knight, J. Davidson, and S. Behrens, "Energy options for wireless sensor nodes," *Sensors*, vol. 8, no. 12, pp. 8037 – 8066, 2008.

[70] S. Ulukus, A. Yener, E. Erkip, O. Simeone, M. Zorzi, P. Grover, and K. Huang, "Energy harvesting wireless communications: A review of recent advances," *IEEE J. Sel. Areas Commun.*, vol. 33, no. 3, pp. 360–381, 2015.

[71] H. Wang, J.-D. Park, and Z. J. Ren, "Practical energy harvesting for microbial fuel cells: a review," *Environ. Sci. Technol.*, vol. 49, no. 6, pp. 3267–3277, 2015.

[72] P. Kopola, T. Aernouts, R. Sliz, S. Guillerez, M. Ylikunnari, D. Cheyns, M. Välimäki, M. Tuomikoski, J. Hast, G. Jabbour, R. Myllylä, and A. Maaninen, "Gravure printed flexible organic photovoltaic modules," *Solar Energ. Mat. Sol. C.*, vol. 95, no. 5, pp. 1344–1347, 2011.

[73] J. Keskinen, S. Lehtimäki, A. Dastpak, S. Tuukkanen, T. Flyktman, T. Kraft, A. Railanmaa, and D. Lupo, "Architectural modifications for flexible supercapacitor performance optimization," *Electron. Mater. Lett.*, vol. 12, no. 6, pp. 795–803, 2016.

[74] A. M. Österholm, D. E. Shen, A. L. Dyer, and J. R. Reynolds, "Optimization of PEDOT films in ionic liquid supercapacitors: Demonstration as a power source for polymer electrochromic devices," *ACS Appl. Mater. Interfaces*, vol. 5, no. 24, pp. 13 432–13 440, 2013.

[75] V. Ruiz, S. Roldán, I. Villar, C. Blanco, and R. Santamaría, "Voltage dependence of carbon-based supercapacitors for pseudocapacitance quantification," *Electrochim. Acta*, vol. 95, pp. 225–229, 2013.

[76] S. Tuukkanen, M. Välimäki, S. Lehtimäki, T. Vuorinen, and D. Lupo, "Behaviour of one-step spray-coated carbon nanotube supercapacitor in ambient light harvester circuit with printed organic solar cell and electrochromic display," *Sci. Rep.*, vol. 6, p. 22967, 2016.

[77] J. Pörhönen, S. Rajala, S. Lehtimäki, and S. Tuukkanen, "Flexible piezoelectric energy harvesting circuit with printable supercapacitor and diodes," *IEEE T. Electron Dev.*, vol. 61, no. 9, pp. 3303–3308, 2014.

Tampereen teknillinen yliopisto
PL 527
33101 Tampere

Tampere University of Technology
P.O.B. 527
FI-33101 Tampere, Finland

ISBN 978-952-15-3922-0
ISSN 1459-2045